SAND2020-1281PE

Relationship of the Mallat Scattering Transformation (a deep convolutional network) to causal physics and complexity

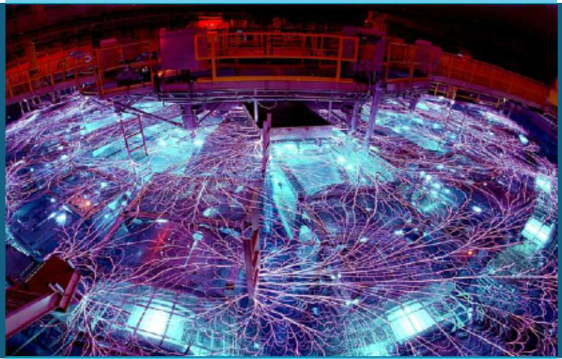

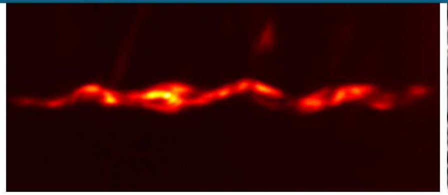

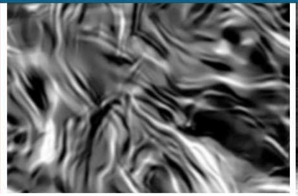

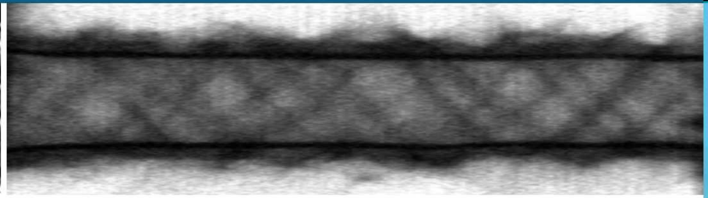

PRESENTED BY

Michael Glinsky

SAND report: http://arxiv.org/abs/1911.02359

Team members

- Sandia National Laboratories
  - Michael Glinsky
  - Thomas Moore (postdoc)
  - Will Lewis (postdoc)
  - Matt Weis
  - Chris Jennings
- College de France
  - Stèphane Mallat
- Enthought Inc.
  - Ben Lasscock
  - Brendon Hall

Connection of MST to causal dynamics (classical & QFT) and MLDL

- useful for Machine and Deep Learning of causal physics
- important tool for theoretical physics, for the analysis of:
  - turbulence, emergent behavior, self-organization, and renormalization

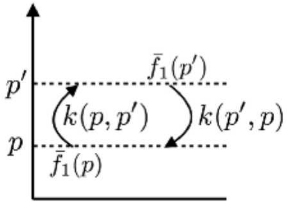

$$\frac{\partial \bar{f}_1(p)}{\partial t} - \frac{\partial \bar{f}_{\text{source}}(p)}{\partial t} \backsim \int dp' \ \bar{f}_2(p',p) - \bar{f}_2(p,p') = \int dp' \ \bar{f}_1(p')\, k(p',p) - \bar{f}_1(p)\, k(p,p')$$

classical kinetic

where $\quad k(p,p') \equiv \dfrac{\bar{f}_2(p,p')}{\bar{f}_1(p)}$

field theoretical

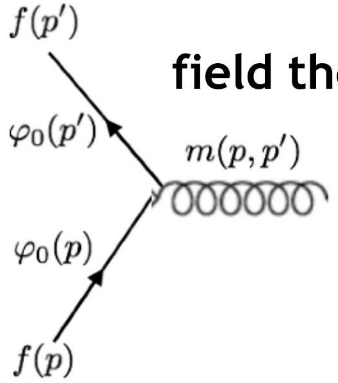

$$S_1(p) = S_1(|f\rangle) = |f \star \psi_p| \star \phi = \bar{f}_1(p) = \varphi_0(p)$$

state of system

$$S_2(p,p') = S_2(|f\rangle) = ||f \star \psi_p| \star \psi_{p'}| \star \phi = \bar{f}_2(p,p') = 1/m(p,p')$$

QFT S-matrix

deep convolutional network

kinetic distribution function

Feynman diagram

transition rates

Resulting practical applications

- deep representation for MLDL of causal physical systems
  - classification (characterization)
  - regression
  - surrogate construction of causal physical system evolution
    - from ensemble of states that sample transition kernel and current state
- metric of image morphology (complexity)
  - compare simulations to experimental images, cross experimental images
  - estimate the parameters of the images with uncertainty via a shallow (linear) regression
  - sophisticated background subtraction

Roadmap

- construction of Mallat Scattering Transformation (MST) as a deep convolutional network with pre-determined weights
- MST from the classical perspective
  - manifold-safe Wigner-Weyl transformation of the density operator
    - bi-transformation because operators have inputs and outputs
    - on manifold with spherical topology can use Fourier kernel and reduces to bi-spectral transformation
  - Generalized Master Equation
- MST from the Quantum Field Theory (QFT) perspective
  - generalized Green's function or S-matrix
  - Feynman diagram of quantum fluctuation averaged classical action and renormalized mass
- applications
  - image classification
  - experimental to computer simulation image comparison
    - advanced background subtraction
  - parametric model estimation of experimental images with uncertainty via regression
  - future direction MLDL of causal physics
    - surrogates of PDE evolution
    - identification of emergent behavior

What is a Wavelet Transform?

- Wavelet Transform, $\mathcal{W}$
  - Convolutions of a signal with dilated Mother Wavelets, $\psi_\lambda(t)$ (i.e. a bank of band-pass filtered signals)
  - $\psi_\lambda(t'-t)$ consists of dilations and translations of the Mother Wavelet $\psi(t)$

1-D Wavelet Trasform

$$x[\lambda](t) = \mathcal{W}\{x(t)\} = x \star \psi_\lambda = \int x(t')\psi_\lambda(t'-t)dt'$$

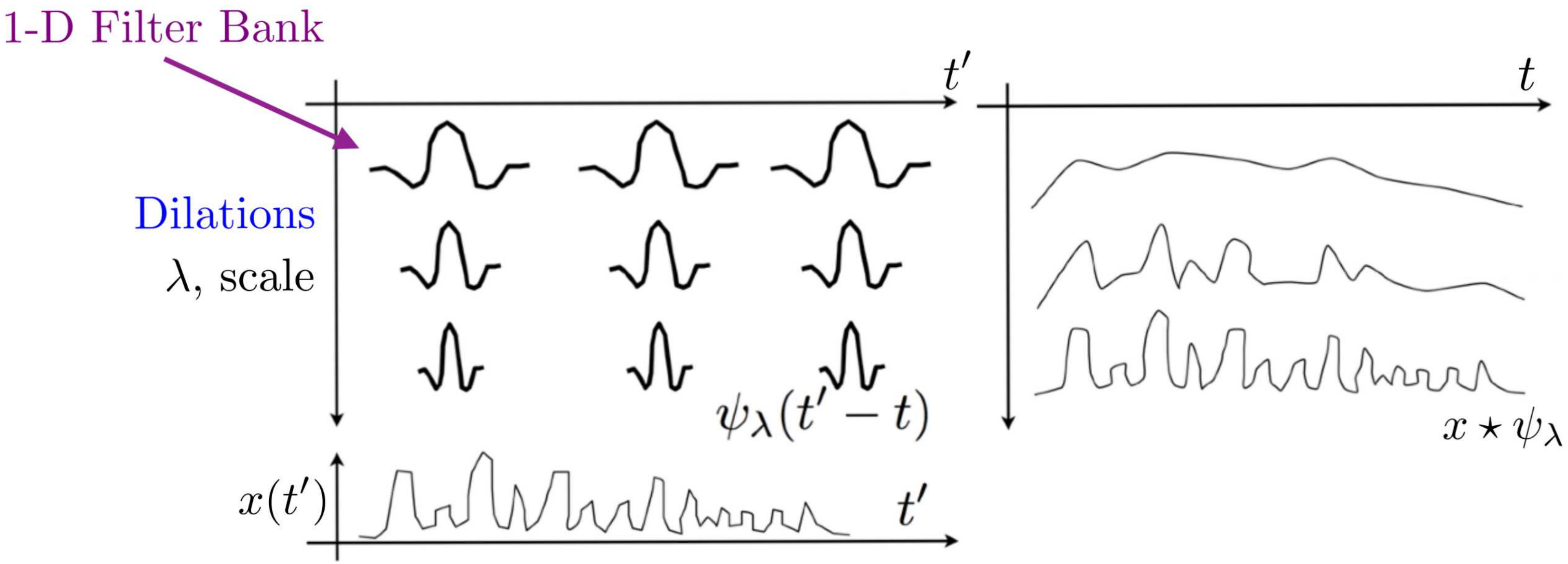

Animation of calculation of Wavelet Transformation convolution

$$x(\lambda, t) = \mathcal{W}\{x(t)\} = x \star \psi_\lambda = \int x(t')\psi_\lambda(t' - t)dt'$$

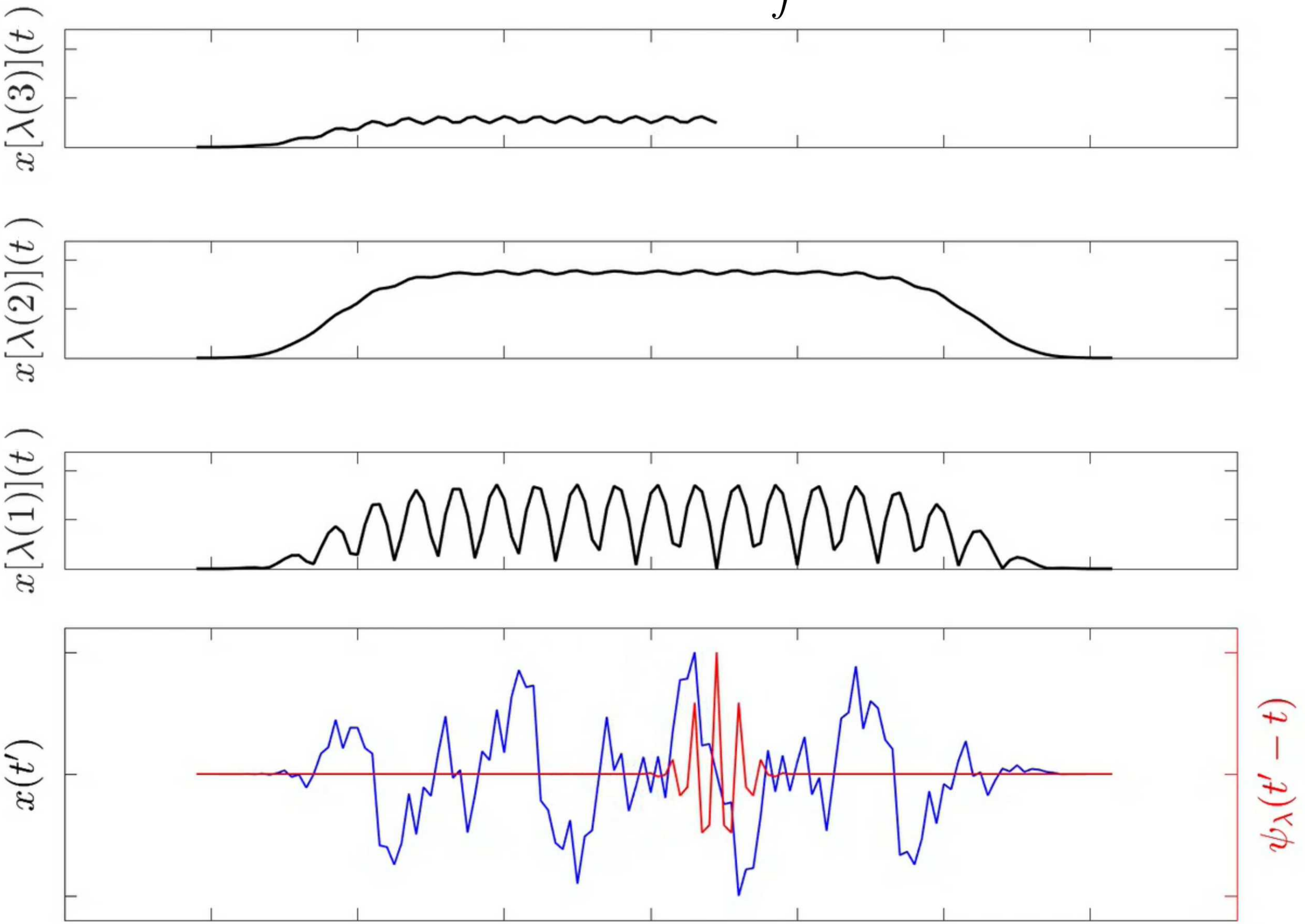

Wavelet Transformations can be iterated

- Wavelet Transform, $\mathcal{W}$
  - convolutions of a signal with dilated Mother Wavelets, $\psi_\lambda(t)$ (i.e. a bank of band-pass filtered signals)
  - $\psi_\lambda(t'-t)$ consists of dilations and translations of the Mother Wavelet $\psi(t)$
  - because $x[\lambda](t)$ is a function of time we can take its Wavelet Transform

Wavelet Transform of a Wavelet Transform

$$x[\lambda_1, \lambda_2](t) = |x \star \psi_{\lambda_1}| \star \psi_{\lambda_2}$$

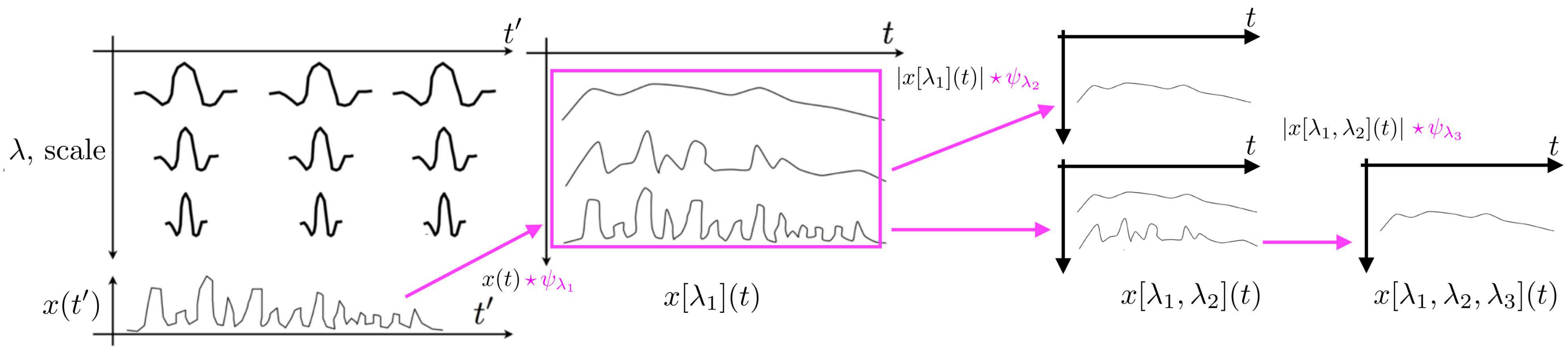

The Mallat Scattering Transform (MST)

[Mallat 2012; Bruna and Mallat 2013; Mallat 2016]

$$\boxed{S_m[\lambda \equiv \sum_{n=1}^{m} \lambda_n]x = \underbrace{\tilde{W}_m\{x(t)\}}_{} = |||x \star \psi_{\lambda_1}| \star \psi_{\lambda_2}| \cdots \star \psi_{\lambda_m}| \star \phi}$$

Mallat Scattering Transform, $\tilde{\mathcal{W}}$

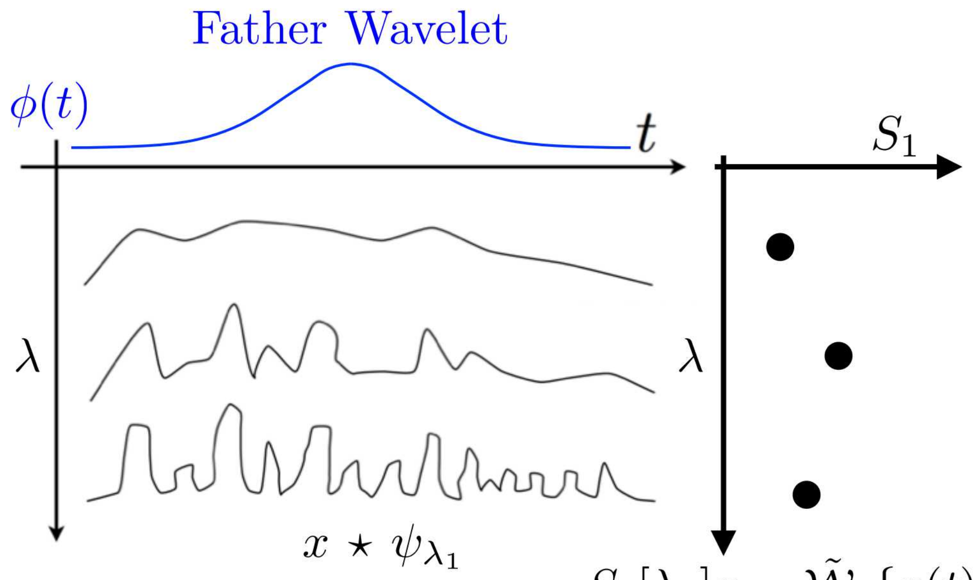

$$S_1[\lambda_1]x = \tilde{\mathcal{W}}_1\{x(t)\} = |x \star \psi_{\lambda_1}| \star \phi$$

Our systems are diffeomorphisms

- Liouville equation
- BBGKY hierarchy
- Master equation
- Vlasov equation
- Boltzmann equation
- multi fluid equations
- Navier-Stokes equations
- MHD equations
- Heat diffusion
- Radiation transport
- Quantum field theory
- Quantum mechanics
- Maxwell's equations
- Newton's equations
- etc.

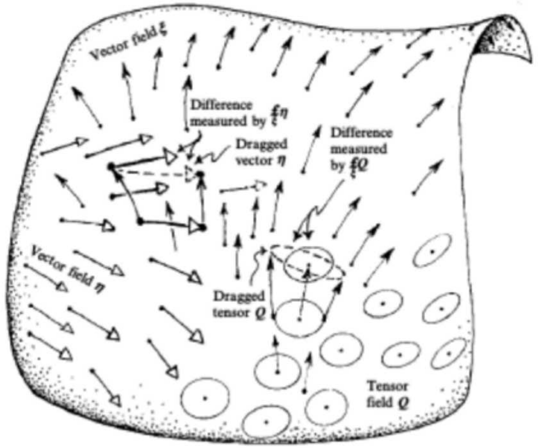

that is, advection by a vector field

$$\boxed{\frac{\partial \rho^{(N)}}{\partial t} + \mathscr{L}_{u^{(N)}} \rho^{(N)} = 0 \qquad \textbf{Generalized Liouville Equation}}$$

$\rho^{(n)} \equiv f_n \tau^{(n)} =$ n-particle distribution form, where $\tau^{(n)} \equiv \prod_{i=1}^{n} \wedge \omega_i$

$\mathrm{i}_{u^{(n)}} \omega^{(n)} = -\mathrm{d}H^{(n)}$, where $\omega^{(n)} \equiv \sum_{i=1}^{n} \omega_i$

$$\boxed{\frac{\partial \rho^{(n)}}{\partial t} + \mathscr{L}_{u^{(n)}} \rho^{(n)} = -n_0 \int_{T^*M} \mathscr{L}_{u^{(n)}_{\mathrm{int}}} \rho^{(n+1)} \qquad \textbf{Generalized BBGKY Hierarchy}}$$

$u^{(n)}_{\mathrm{int}} \equiv \sum_{i=1}^{n} u_{i,n+1}$

this is why Lipschitz continuity (invariance under diffeomorphism, deformation, or advection) is such a big deal

$$\boxed{\rho = \text{statistical distribution or QFT state}}$$

Relation of MST to Generalized Master Equation: ideas of Bogoliubov

f_1 relaxes at dynamic rate $= \Omega$

$\bar{f}_1$ evolves at collisional rate $= \dfrac{d\Omega/dt}{\Omega} \ll \Omega$

f_2 relaxes at collision rate

$\bar{f}_2$ evolves at correlation rate $= \dfrac{d^2\Omega/dt^2}{\Omega^2} \ll \dfrac{d\Omega/dt}{\Omega} \ll \Omega$

pullback of first two equations in BBGKY hierarchy,

$$\frac{\partial f_1}{\partial t} + \{f_1, H_1\} = -n_0 \int dp_2\, dq_2\, \{f_2, H_{12}\}$$
$$\frac{\partial f_2}{\partial t} + \{f_2, H_1 + H_2 + H_{12}\} = -n_0 \int dp_3\, dq_3\, \{f_3, H_{13} + H_{23}\}$$

can be reduced to, assuming the separation of rates,

$$\boxed{\frac{\partial \bar{f}_1(p)}{\partial t} \backsim \int dp'\ \bar{f}_2(p', p) - \bar{f}_2(p, p') \qquad \textbf{Generalized Master Equation}}$$

$$= \int dp'\ \bar{f}_1(p')\, k(p', p) - \bar{f}_1(p)\, k(p, p') \qquad k(p, p') \equiv \frac{\bar{f}_2(p, p')}{\bar{f}_1(p)}$$

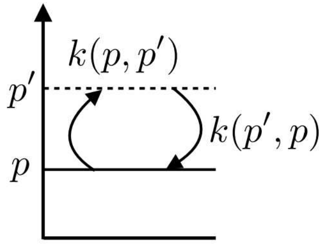

Relation of MST to Generalized Master Equation: manifold safe Wigner-Weyl transformation

Wigner-Weyl transformation takes operators to/from classical phase space (1927).
The Key is a modified Wigner-Weyl transform that is manifold safe.
Need a local Fourier kernel (Mother Wavelet) with a partition of unity (Father Wavelet).

$$\text{modified Wigner map} = \tilde{W}[\hat{A}] \equiv \int ds\, \psi_p^*(-s) \left\langle q+s \middle| \hat{A} \middle| q-s \right\rangle \psi_p(s) = A(q,p)$$

$$\text{modified Wigner function} = \tilde{W}[\hat{\rho}] = \tilde{W}[\,|f\rangle\langle f|\,] = |f \star \psi_p|^2 = \tilde{W}_f(q,p)$$

Now we can identify and calculate,

$$\bar{f}_1(p) \equiv \mathrm{E}(\tilde{W}[\hat{f}]) = |f \star \psi_p| \star \phi = S_1[p]f$$

$$\bar{f}_2(p,p') \equiv \mathrm{E}(\tilde{W}[\hat{f}\hat{f}]) = ||f \star \psi_p| \star \psi_{p'}| \star \phi = S_2[p,p']f$$

This is the Mayer Cluster expansion on the manifold.

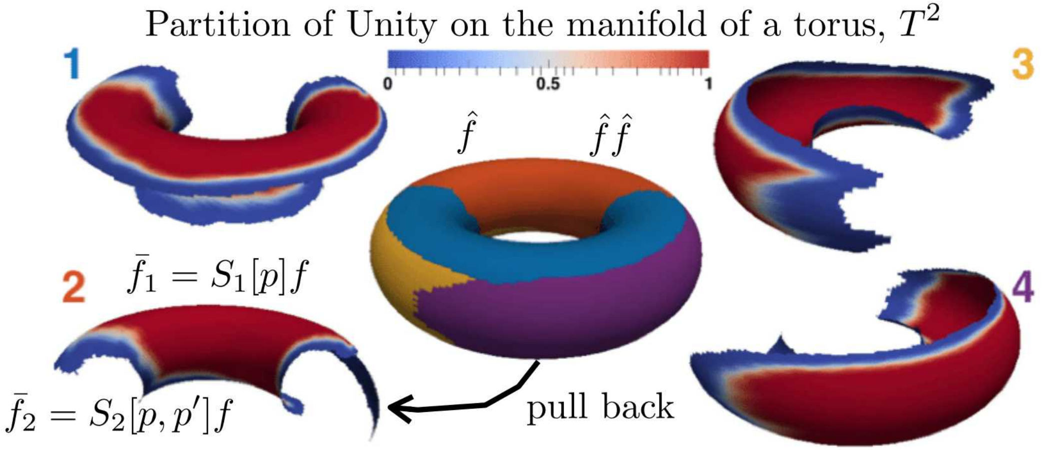

MST as the S-matrix: an alternative dynamical interpretation (I)

From the Lagrangian perspective define the generating function:

$$Z[J] = N \int [df(p)]\, \mathrm{e}^{(i/\hbar)\, S_0[f(p)] + (i/\hbar) \int dp\, J(p)\, f(p)}$$

the connection to the canonical formulation is:

$$S_m(|f\rangle) = \mathrm{E}(T_p(\hat{f}(p_1)\ldots\hat{f}(p_m))\, F(f)) = ||f \star \psi_{p_1}| \cdots \star \psi_{p_m}| \star \phi = \frac{1}{Z[J]} \frac{\delta}{\delta J(p_1)} \cdots \frac{\delta}{\delta J(p_m)} Z[J]\bigg|_{J=0}$$

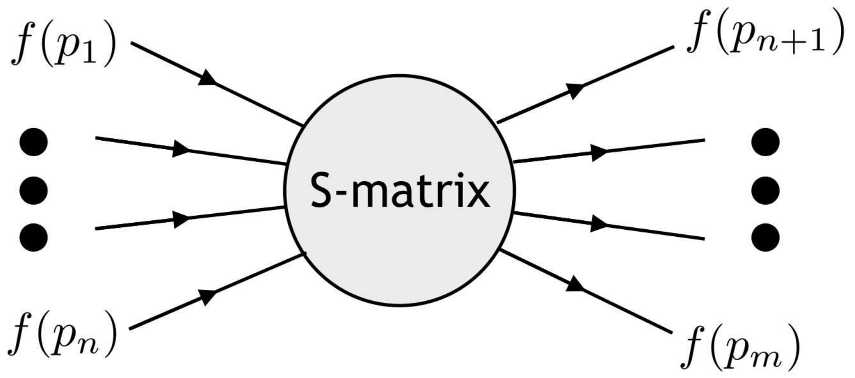

scattering cross section
generalized Green’s function

MST as the S-matrix: an alternative dynamical interpretation (II)

define the effective action through Legendre transform:

$$S[\varphi(p)] = -\ln Z[J] + \int dp\, J(p)\, \varphi(p)$$

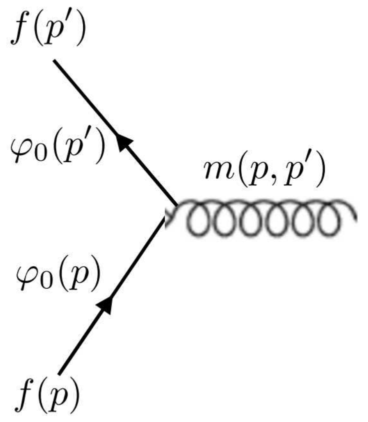

expanding in S and φ it can be shown that:

$$S_1(|f\rangle) = |f \star \psi_p| \star \phi = \mathrm{E}(\hat{f}(p)\, F(f)) = \frac{1}{Z[J]} \frac{\delta Z[J]}{\delta J(p)}\bigg|_{J=0} = \varphi_0(p) =$$

classical action averaged over fluctuations as a function of inverse renormalization scale $= \bar{f}_1(p)$

$$S_2(|f\rangle) = ||f \star \psi_p| \star \psi_{p'}| \star \phi = \mathrm{E}(\hat{f}(p)\, \hat{f}(p')\, F(f)) = \frac{1}{Z[J]} \frac{\delta^2 Z[J]}{\delta J(p) \delta J(p')}\bigg|_{J=0} = \frac{1}{m(p,p')} =$$

two state scattering cross section (scale dependent renormalization mass) as a function of initial and final inverse renormalization scale $= \bar{f}_2(p,p')$

Physical inspiration: self organization or inverse turbulent MHD cascade of MagLIF implosions on Z-machine at Sandia National Laboratories

x-ray self emission of 0.25 gm/cc deuterium @ 2-3 keV

no Bz

high resolution (15-20 microns)

low resolution (60 microns)

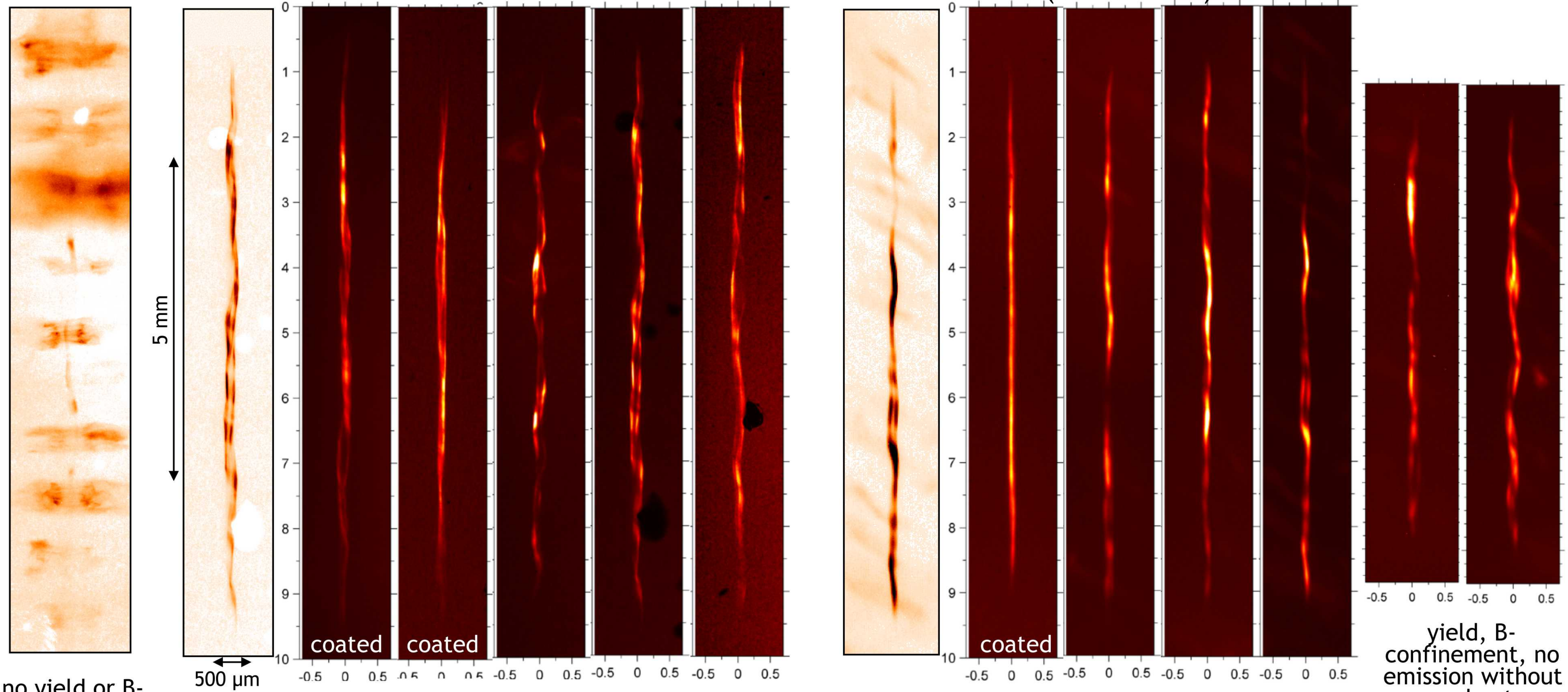

no yield or B-confinement or bulk convergence

diameter ranges from 120 to <23 microns, CR from 38 to >200

yield, B-confinement, no emission without preheat

Construction of synthetic model

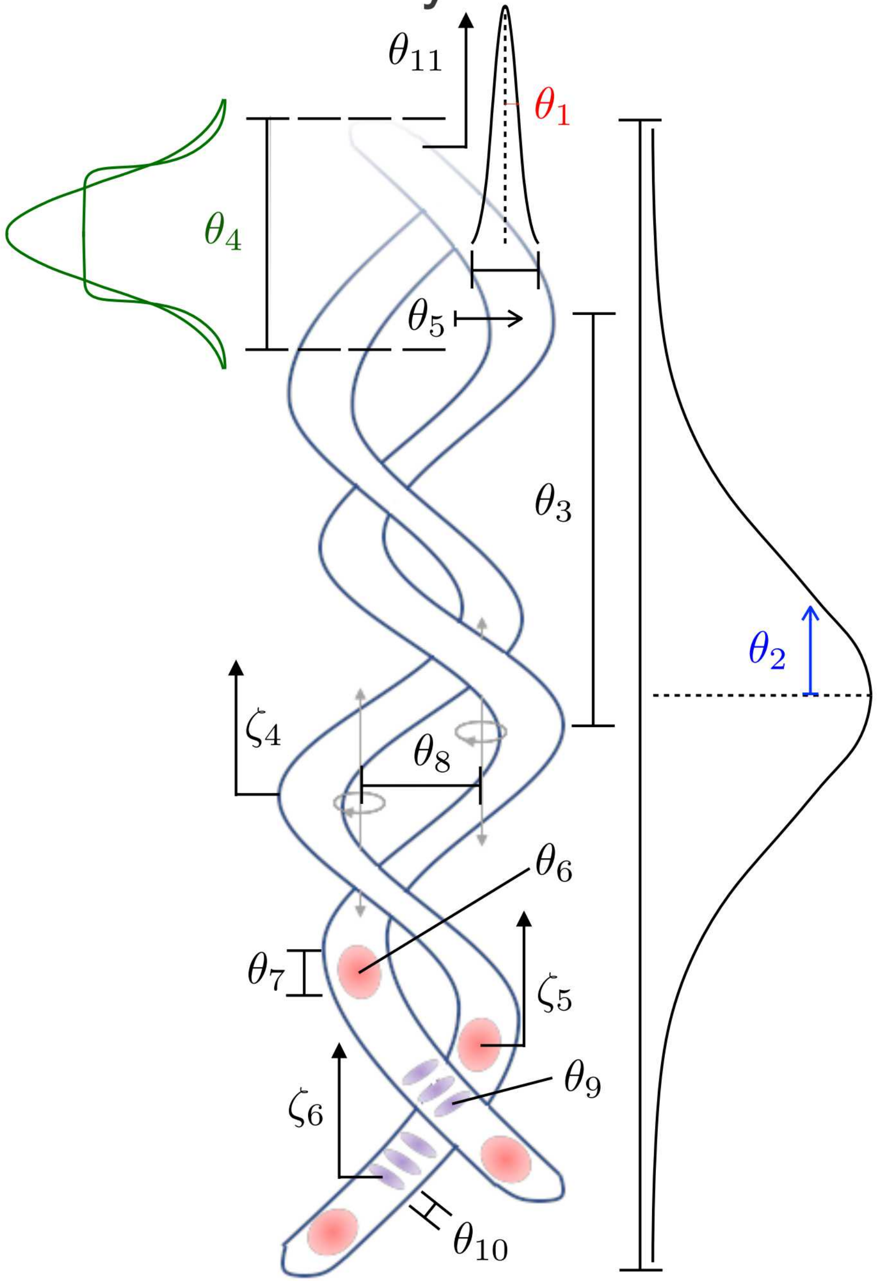

Model Parameters

θ_1 = thickness
θ_2 = length
θ_3 = MRT wavelength
θ_4 = order of axial super Gaussian
θ_5 = amplitude of radial perturbations
θ_6 = amplitude of large-wavelength axial brightness perturbations
θ_7 = mode number of large-wavelength axial brightness perturbations
θ_8 = strand separation
θ_9 = amplitude of small-wavelength axial brightness perturbations
θ_{10} = mode number of small-wavelength axial brightness perturbations
θ_{11} = relative strand phase

Stochastic Parameters

ζ_1 = background noise
ζ_2 = signal noise
ζ_3 = amplitude of signal
ζ_4 = radial perturbation phase shift
ζ_5 = large-wavelength axial brightness perturbations phase shift
ζ_6 = small-wavelength axial brightness perturbations phase shift

Classification ensemble

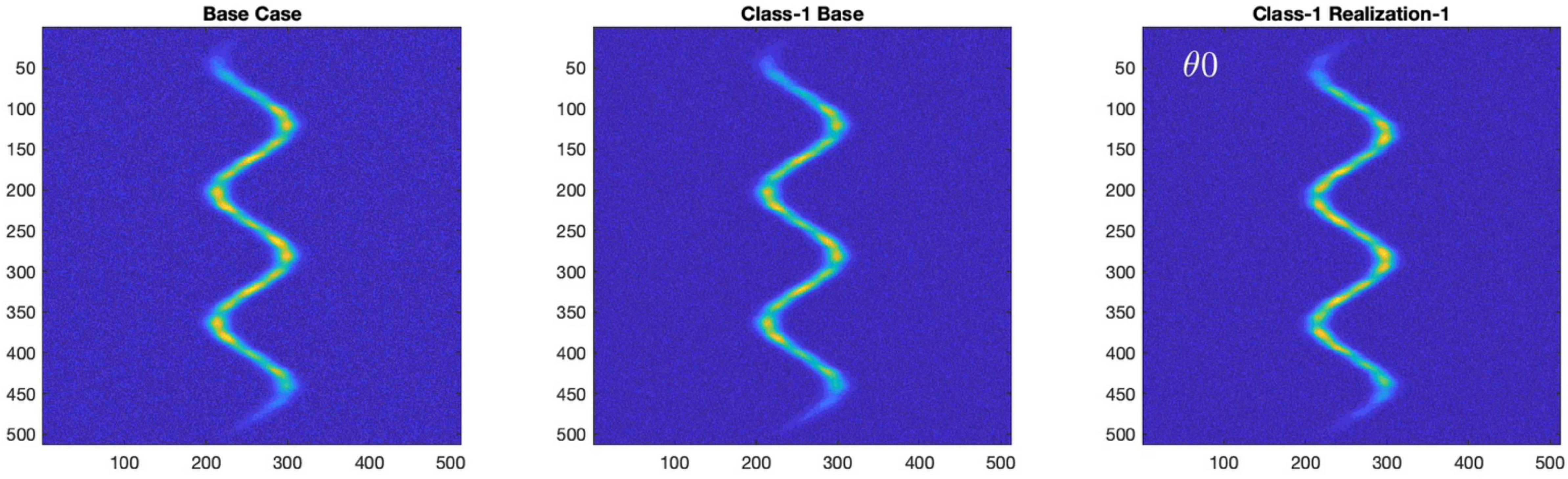

Classification has excellent performance with significant cluster separation in MST space

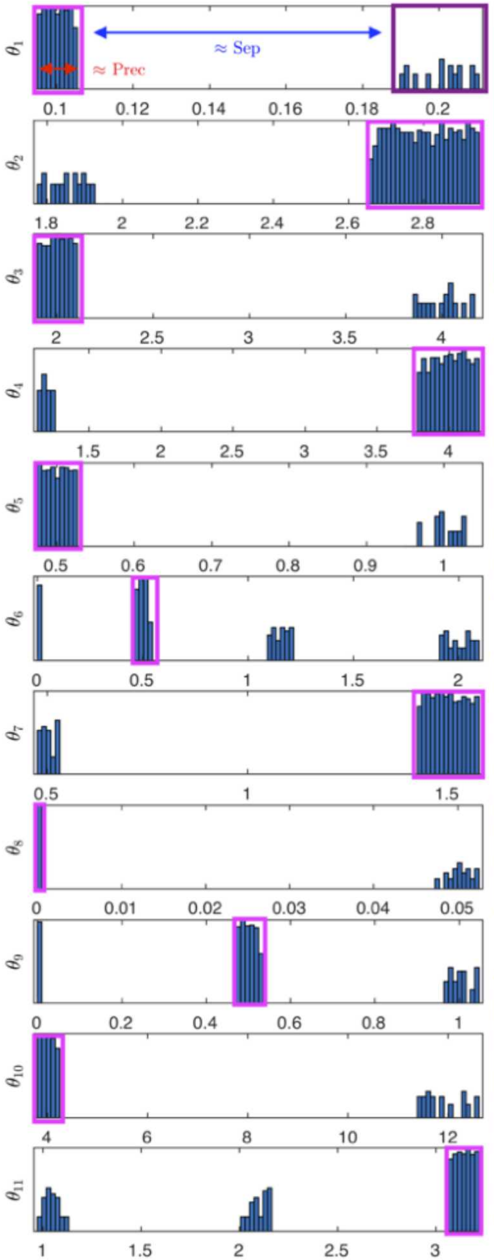

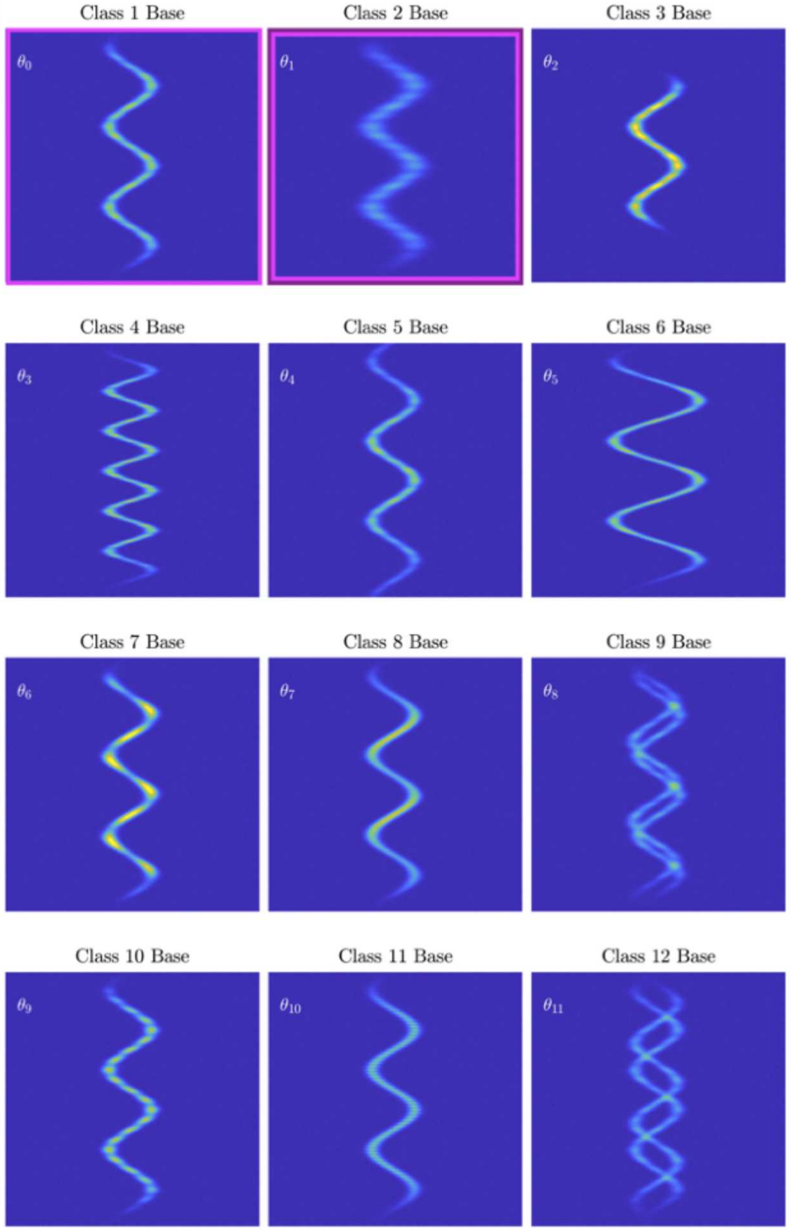

classification confusion matrix (dim=10)

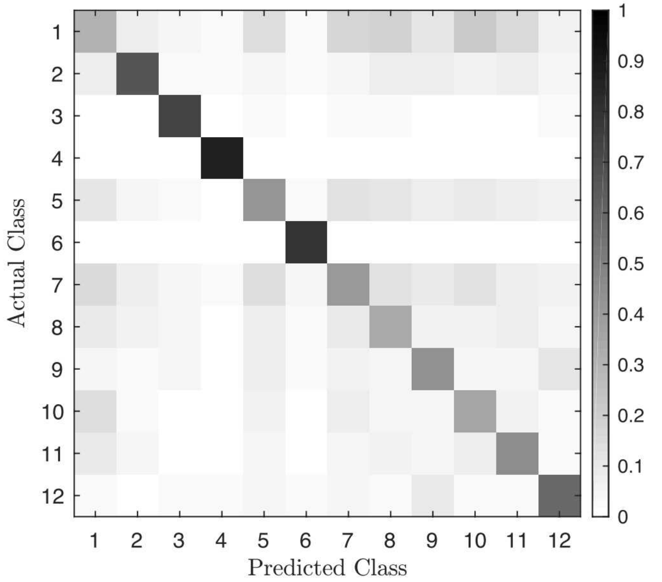

precision = 0.00017

separation = 10

probability of incorrect classification = 0%

Optimization of affine dimension

confusion matrix (different afine dimensions)

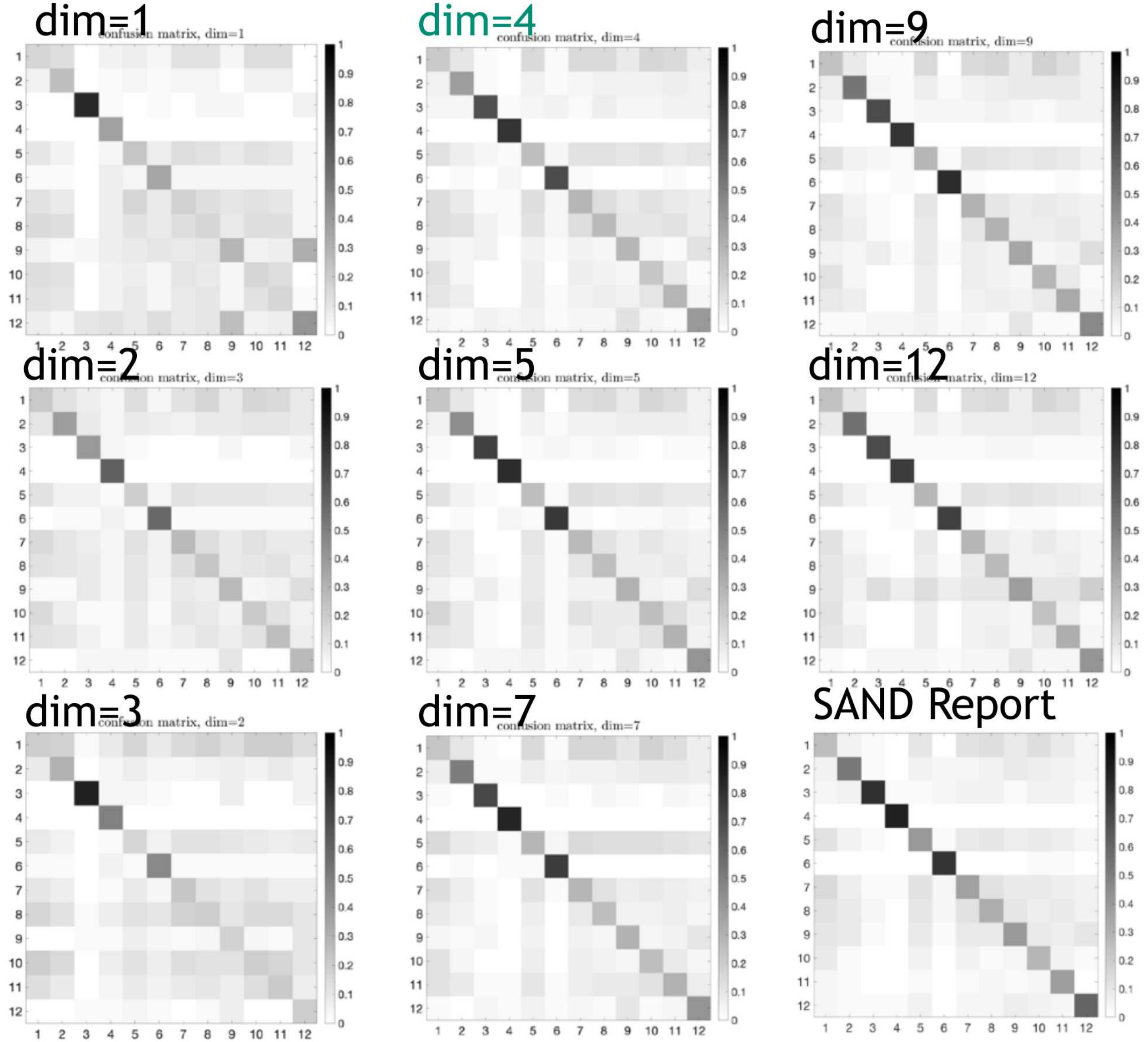

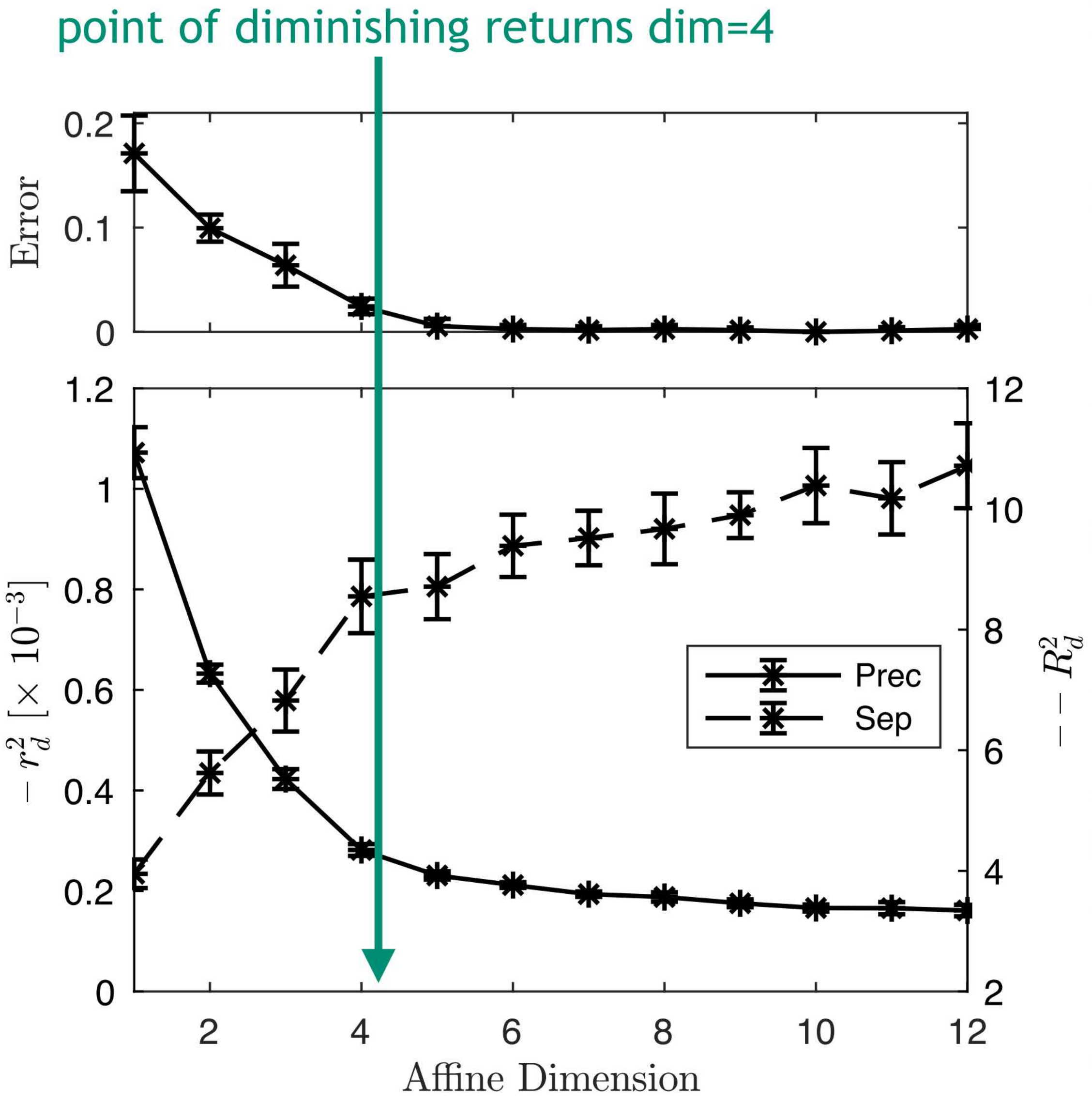

Definition of cluster precision and separation for an affine classifier

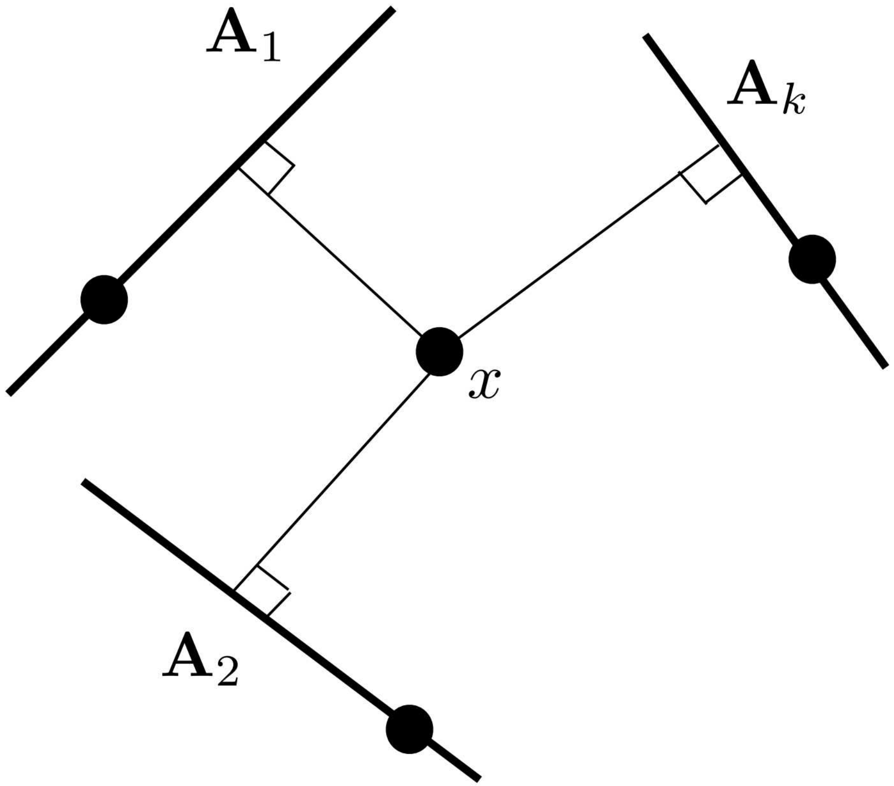

$$x - P_{\mathbf{A}}(x) = x - \sum_{i=1}^{d} < x, A_i >$$

(projection perpendicular to an affine space)

$$\sigma_d^2 = N_C^{-1} \sum_{k=1}^{N_C} \frac{E(||SX_k - P_{\mathbf{A}_k}(SX_k)||^2}{E(||SX_k||^2)}$$

(precision)

$$(\sigma_d^2)_{kl} = \frac{E(||SX_k - P_{\mathbf{A}_l}(SX_k)||^2}{E(||SX_k - P_{\mathbf{A}_k}(SX_k)||^2}$$

(separation factors)

$$\sigma_d^2 = N_C^{-1} \sum_{k=1}^{N_C} \frac{E(\min_{l \neq k}||SX_k - P_{\mathbf{A}_l}(SX_k)||^2}{E(||SX_k - P_{\mathbf{A}_k}(SX_k)||^2}$$

(separation factor)

Comparison of computer simulation to experimental data

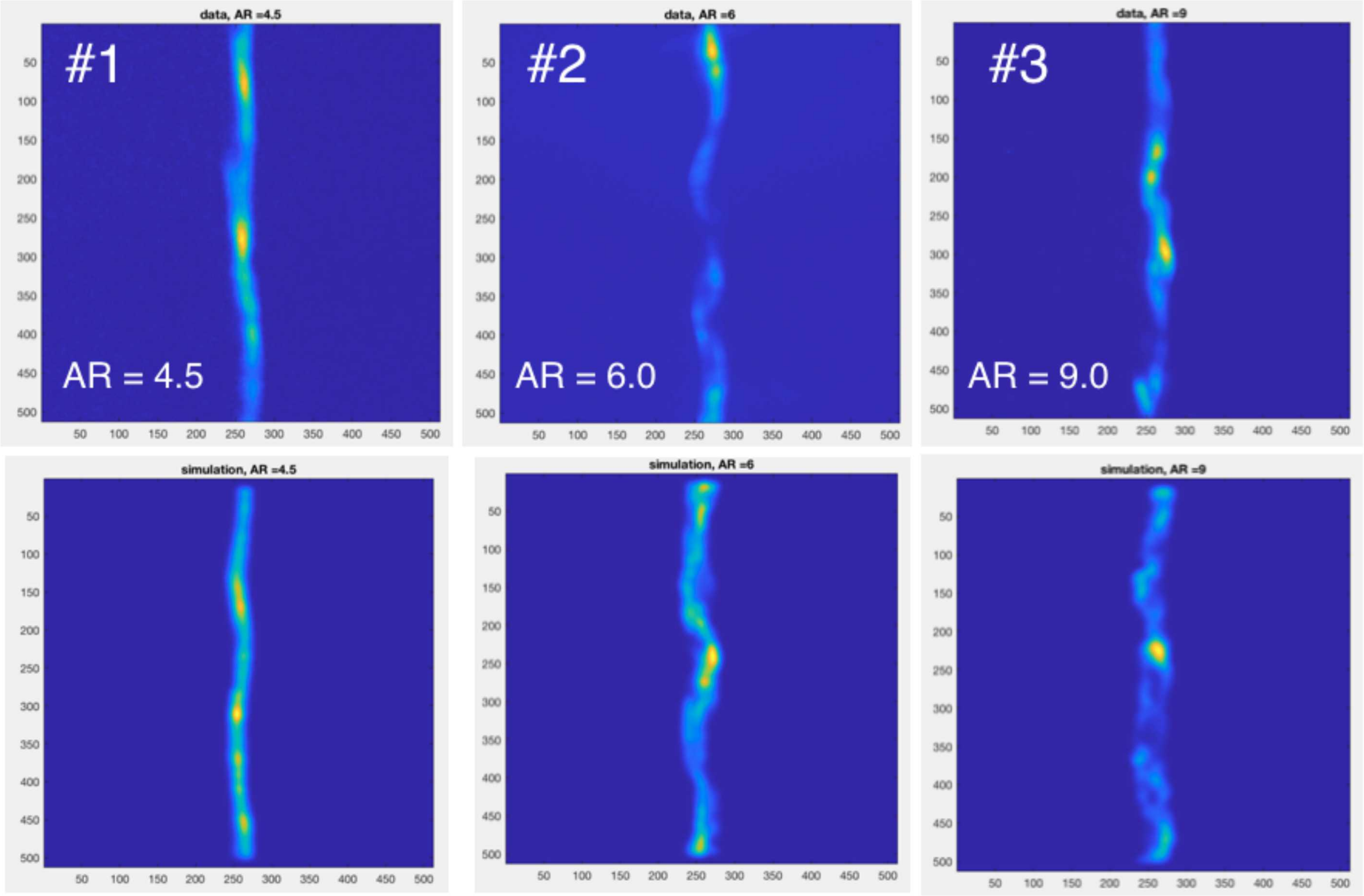

data

sim

Significant distortion between simulation and experiment corrected by MST based background subtraction

solution: first principal component of simulation to data covariance projected out (effective background subtraction)

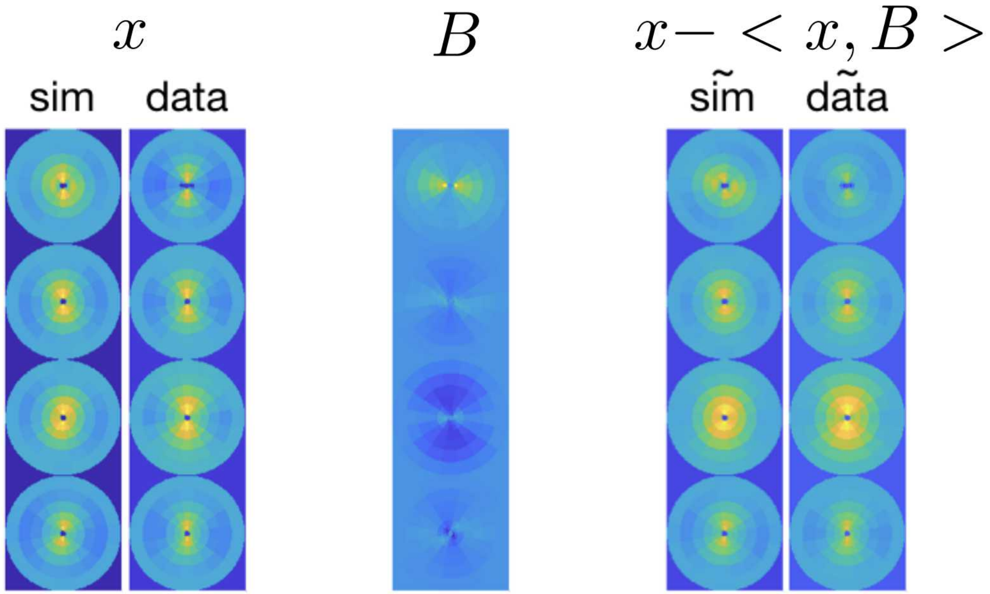

for AR = 4.5

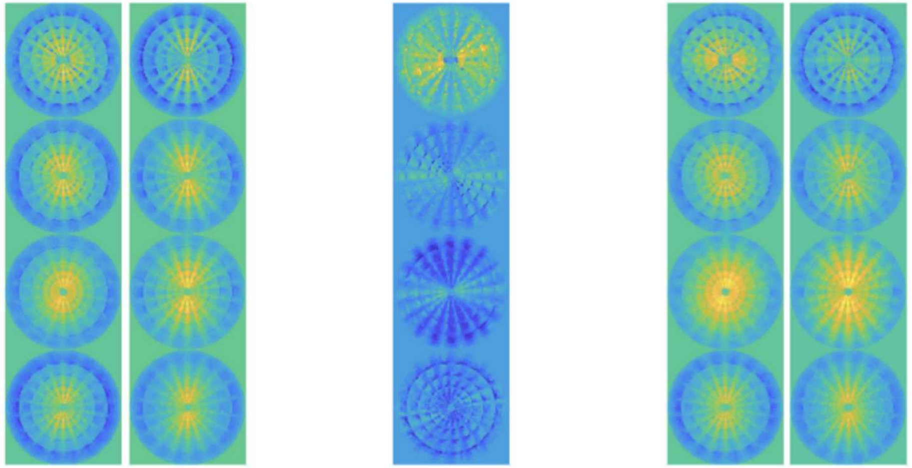

note: cluster precision and separation are improved, by the background subtraction, from 0.40 to 0.08, and from 1.9 to 4.8, respectively

Detailed results of background subtraction

without background subtraction

norm_matrix =

25.2252	21.1719	26.3623
25.4981	42.8571	32.3066

distance_matrix =

5.3270	23.9748	11.7816
12.2075	31.0360	19.4757
9.3089	22.9628	11.3718

separation_matrix =

1.0000	0.5967	1.0734
5.2515	1.0000	2.9331
3.0537	0.5474	1.0000

confusion_matrix =

0.4119	0.3694	0.3784
0.2673	0.2370	0.2333
0.3207	0.3936	0.3883

precision = 0.40
separation = 1.9

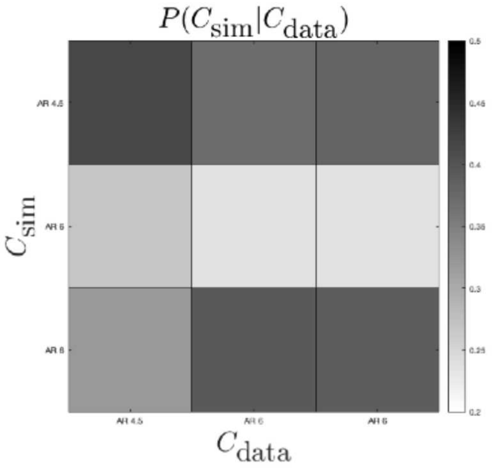

with background subtraction

norm_matrix =

19.9342	20.0386	21.0724
19.4718	20.1892	22.7075

distance_matrix =

5.2315	8.6857	9.0674
7.5048	2.0267	10.8905
9.2881	6.7015	8.8512

separation_matrix =

1.0000	18.3677	1.0494
2.0579	1.0000	1.5139
3.1522	10.9343	1.0000

confusion_matrix =

0.4707	0.1694	0.3632
0.3082	0.5855	0.2587
0.2211	0.2451	0.3781

precision = 0.08
separation = 4.8

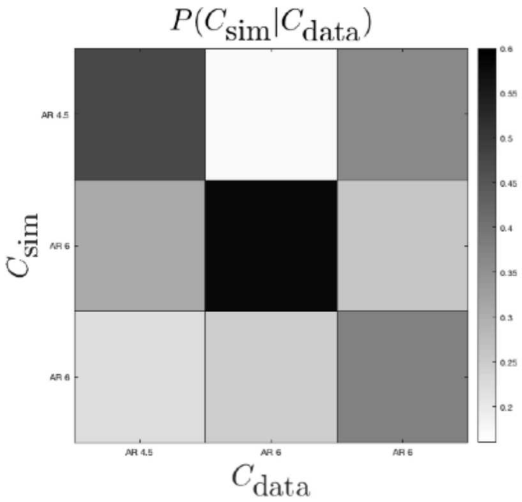

Use of MST as a metric in the quantification of MagLIF stagnation morphology (i.e., self organization or emergent behavior)

- metric qualifies similarities between simulation and experiment
  - enables use of images in Uncertainty Quantification & Verification (UQV)
  - allows quantified statements to be made about morphology
- for example here we can state:
  - the simulations correspond to the matching experiments
  - there is similarity of the AR-9 data to the AR-4.5 simulation

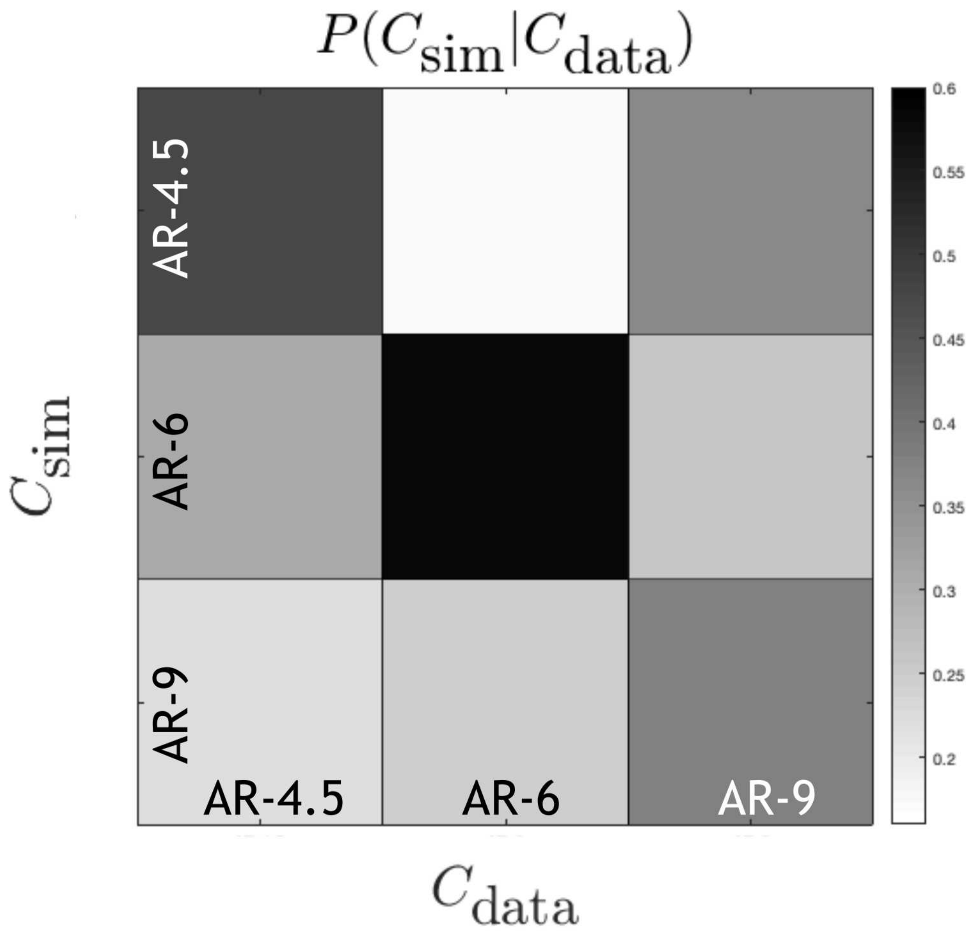

Regression for parameters of stagnation morphology using MST based metric

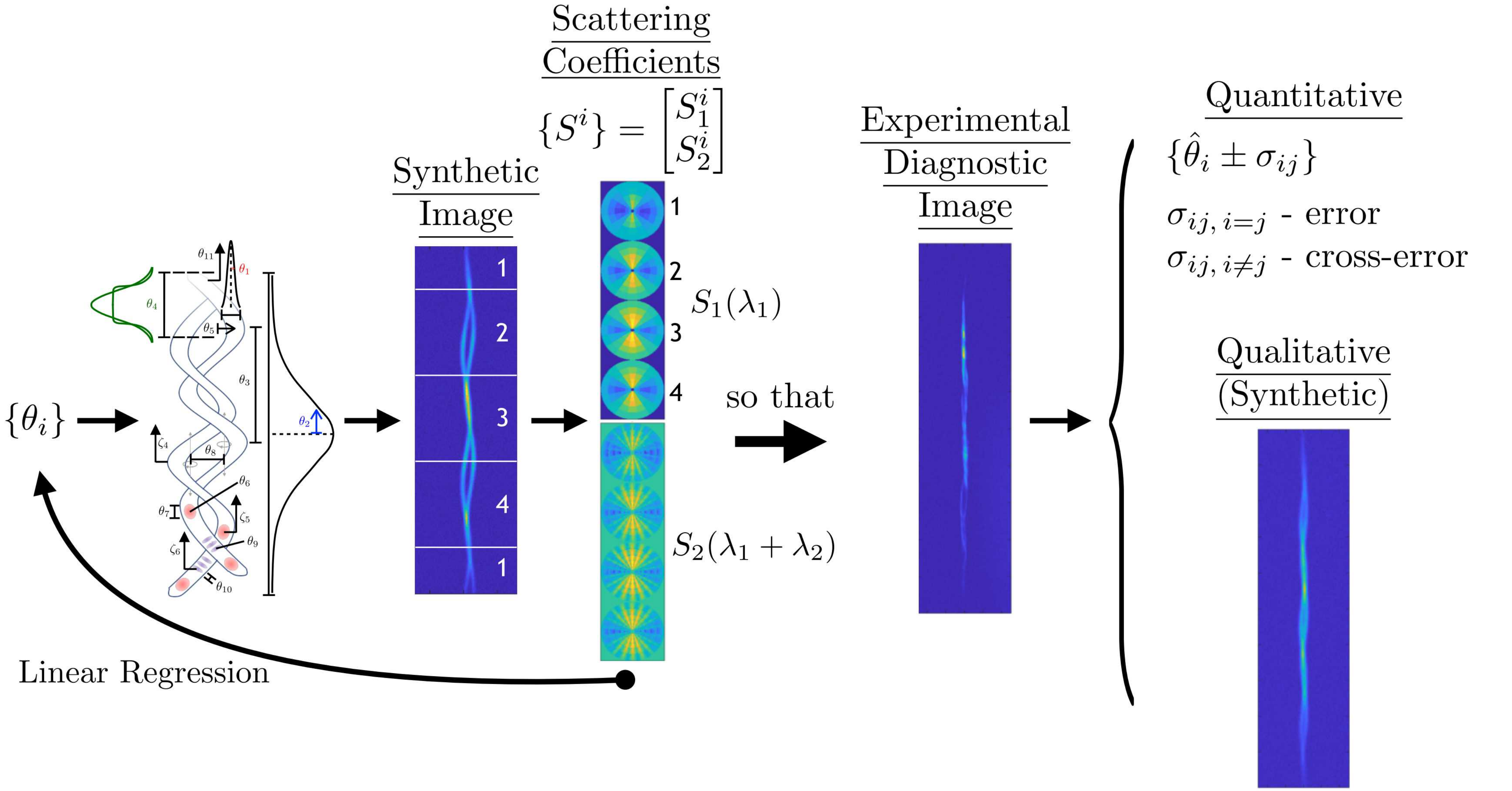

Regression ensemble

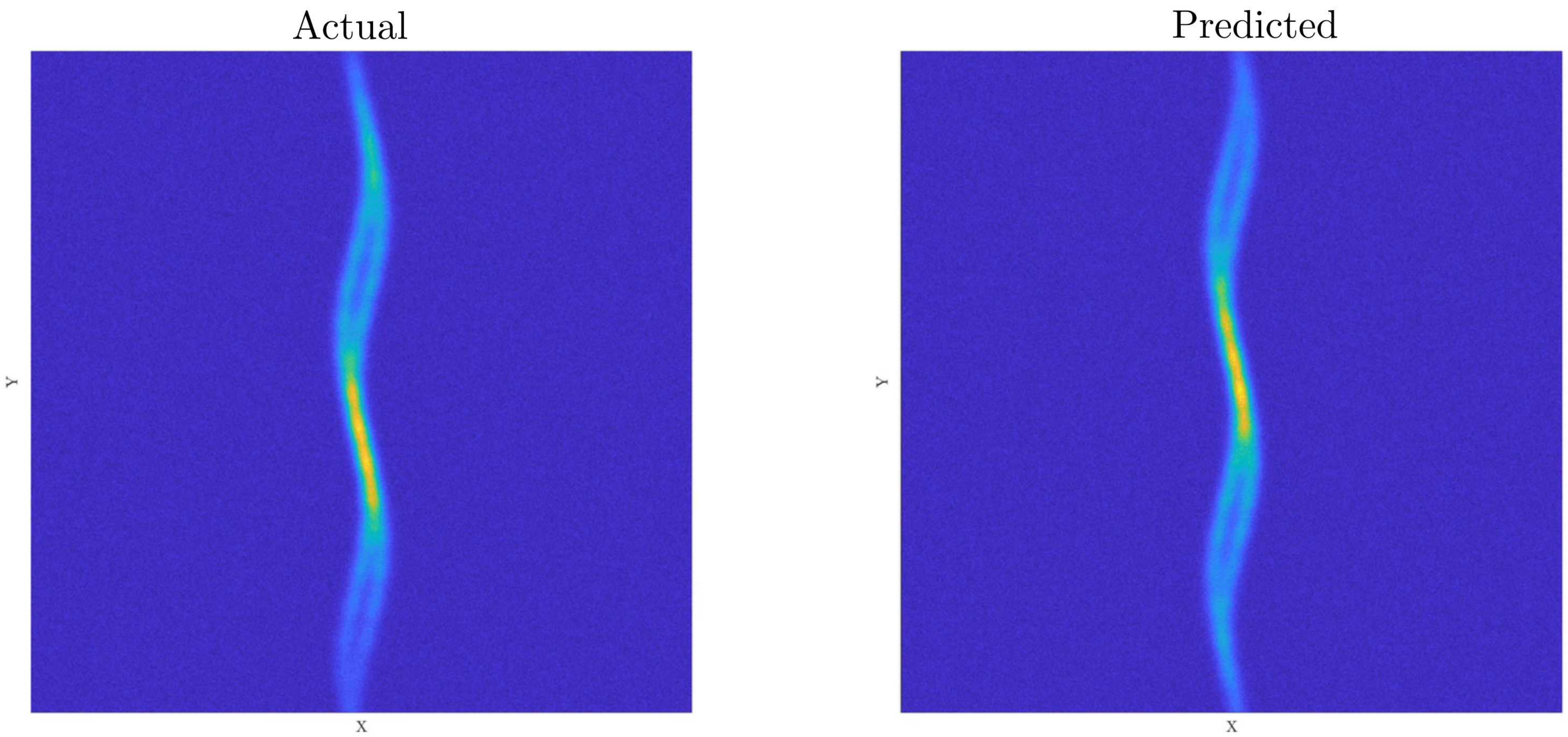

Excellent regression performance

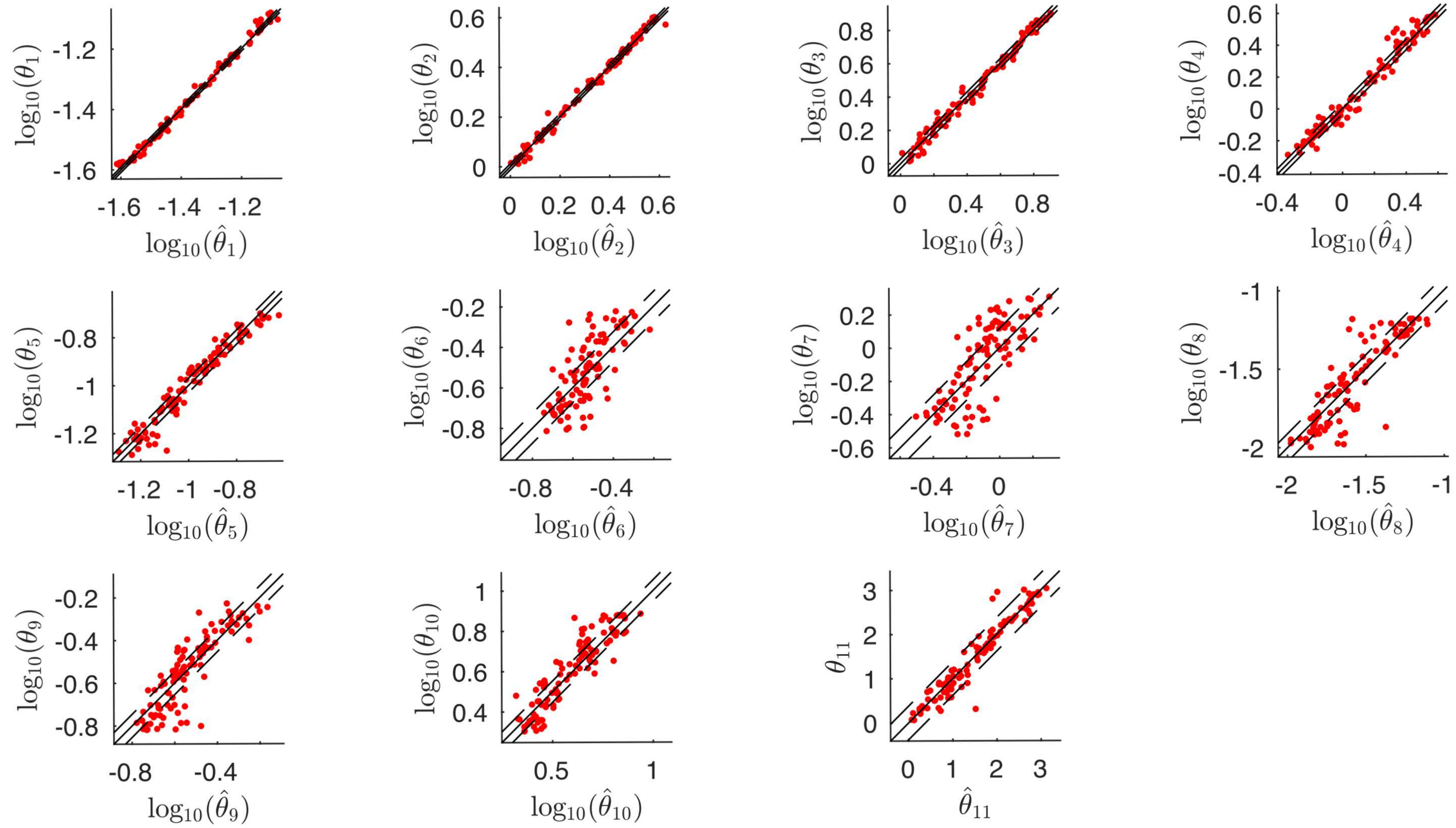

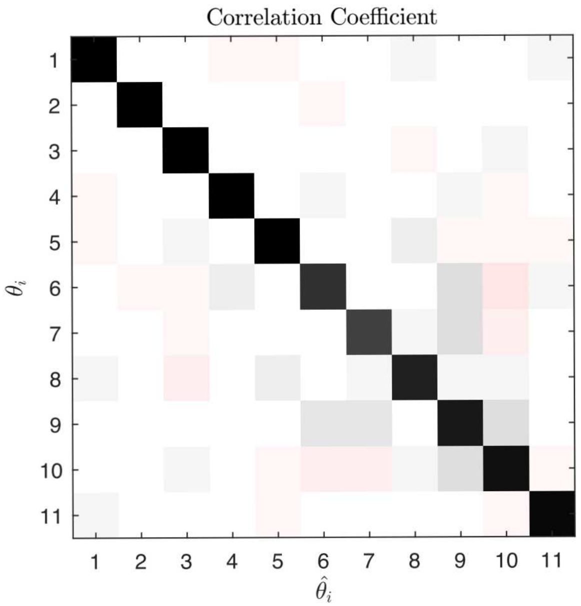

x

Model fit — PCA space

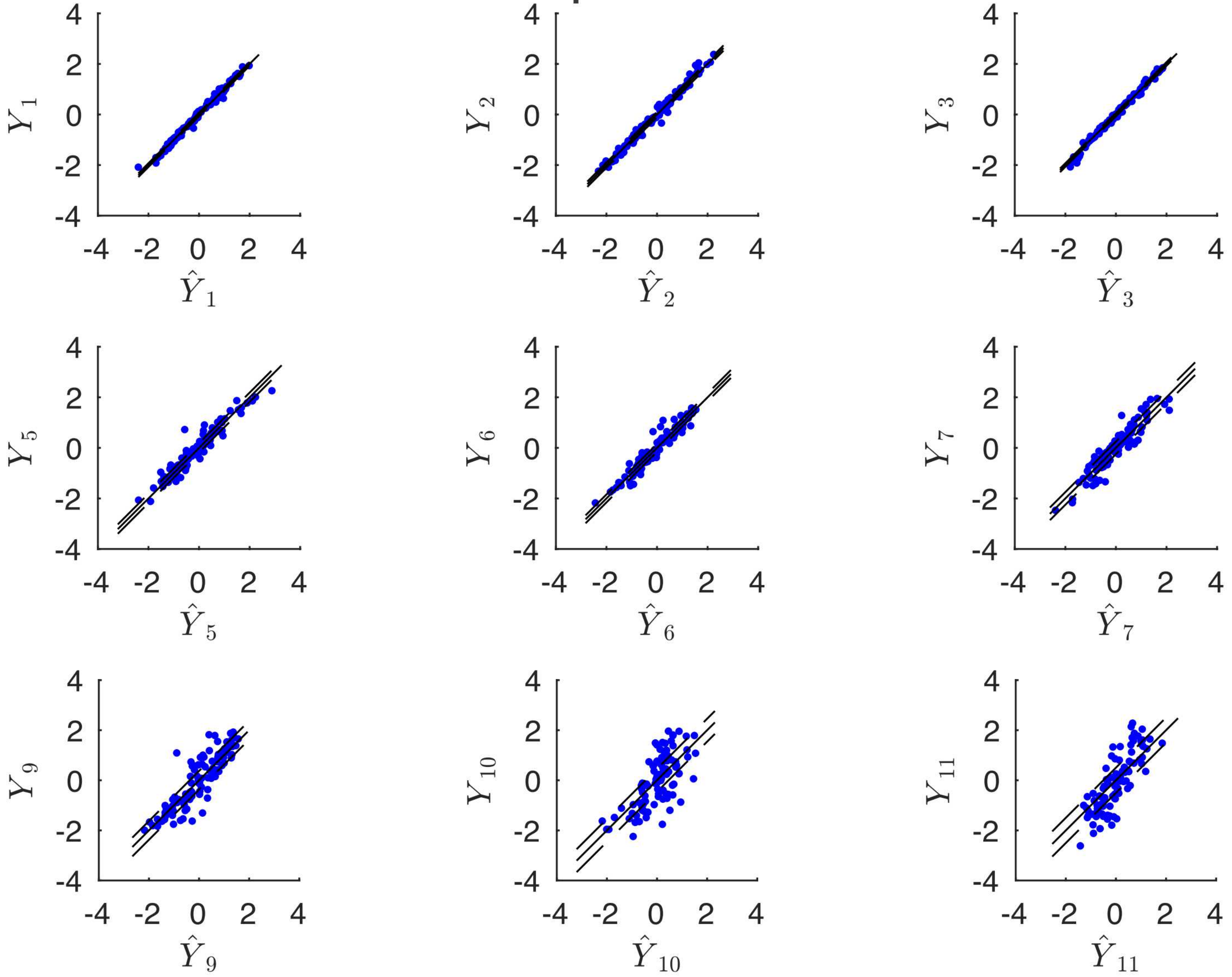

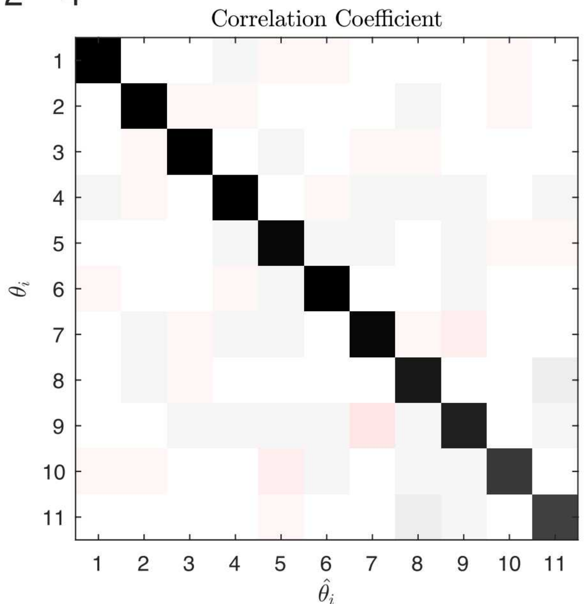

Singular Value Decomposition (SVD)

$$\mathrm{SVD}(\ \mathrm{CCOV}(\theta_i, S_j)) = U\Sigma V^T$$

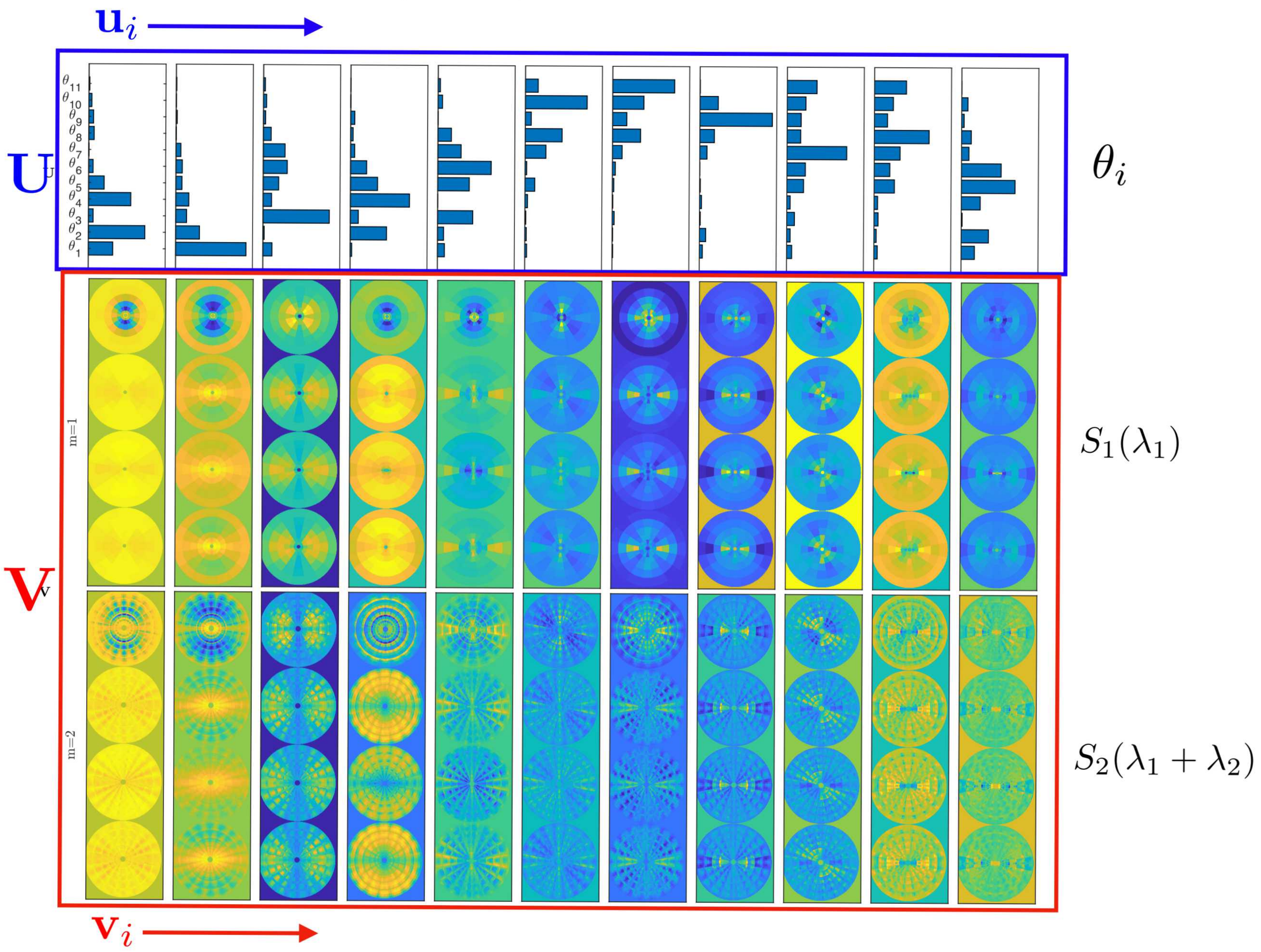

Fit to experimental image (coated AR9) gives estimate of uncertainty

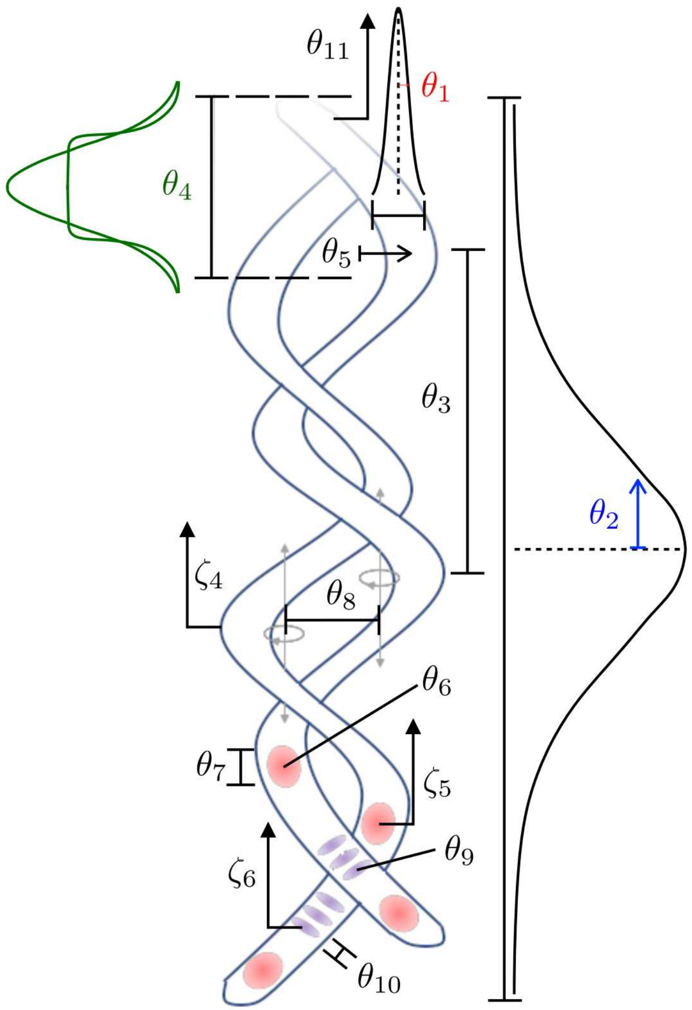

$\theta_1 = 0.0720 + (-0.0034, 0.0036)$

$\theta_2 = 2.2335 + (-0.1425, 0.1546)$

$\theta_3 = 2.1677 + (-0.3083, 0.3509)$

$\theta_4 = 1.5327 + (-0.2560, 0.3003)$

$\theta_5 = 0.0988 + (-0.0145, 0.0176)$

$\theta_6 = 0.1756 + (-0.0568, 0.0838)$

$\theta_7 = 6.8597 + (-3.1944, 5.8555)$

$\theta_8 = 0.0286 + (-0.0107, 0.0175)$

$\theta_9 = 0.2293 + (-0.0579, 0.0805)$

$\theta_{10} = 5.3522 + (-1.3159, 1.7144)$

$\theta_{11} = 0.4819 + (-0.4050, 0.4027)$

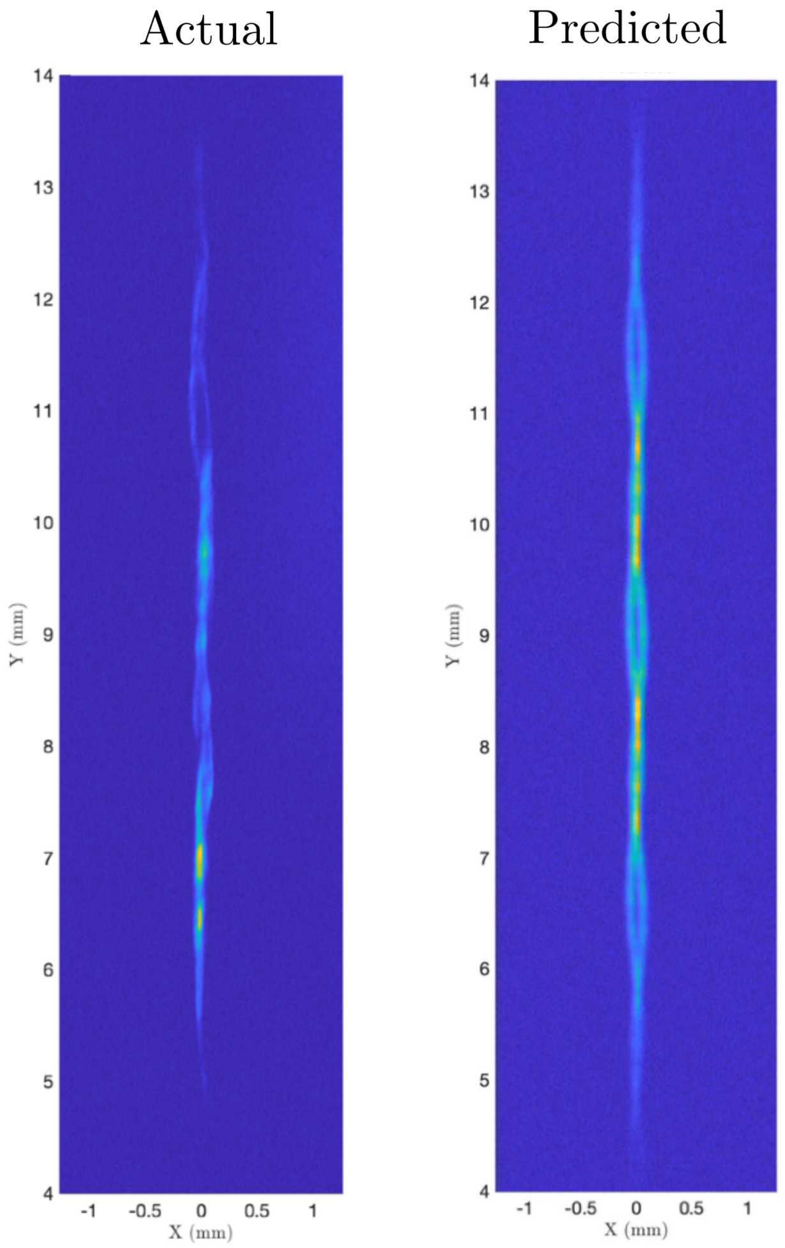

x

Shot Z3236 regression fit uncertainty

	Z3236	Z3289
θ_1	$0.0720 + (-0.0034, 0.0036)$	$0.0651 + (-0.0031, 0.0032)$
θ_2	$2.2335 + (-0.1425, 0.1546)$	$1.4954 + (-0.0950, 0.1013)$
θ_3	$2.1677 + (-0.3083, 0.3509)$	$3.9584 + (-0.5638, 0.6389)$
θ_4	$1.5327 + (-0.2560, 0.3003)$	$0.3120 + (-0.0509, 0.0622)$
θ_5	$0.0988 + (-0.0145, 0.0176)$	$0.1975 + (-0.0282, 0.0337)$
θ_6	$0.1756 + (-0.0568, 0.0838)$	$0.0116 + (-0.0037, 0.0058)$
θ_7	$6.8597 + (-3.1944, 5.8555)$	$79.2478 + (-36.5681, 68.3188)$
θ_8	$0.0286 + (-0.0107, 0.0175)$	$0.0136 + (-0.0051, 0.0084)$
θ_9	$0.2293 + (-0.0579, 0.0805)$	$0.1807 + (-0.0452, 0.0609)$
θ_{10}	$5.3522 + (-1.3159, 1.7144)$	$4.8469 + (-1.1991, 1.5604)$
θ_{11}	$0.4819 + (-0.4050, 0.4027)$	$2.0195 + (-0.4009, 0.4079)$
$\sigma_r(mm)$	$0.0720 + (-0.0034, 0.0036)$	$0.0651 + (-0.0031, 0.0032)$
$\sigma_z(mm)$	$2.2335 + (-0.1425, 0.1546)$	$1.4954 + (-0.0950, 0.1013)$
$\lambda_{helix}(mm)$	$2.8985 + (-0.4123, 0.4692)$	$1.5873 + (-0.2261, 0.2562)$
$R_{\text{helix}}(mm)$	$0.1275 + (-0.0512, 0.0811)$	$0.2111 + (-0.0853, 0.1359)$
$\text{Amp}_{\text{ABS,lf}}$	$0.1756 + (-0.0568, 0.0838)$	$0.0116 + (-0.0037, 0.0058)$
$\lambda_{\text{ABS,lf}}(mm)$	$0.2113 + (-0.0140, 0.0292)$	$0.0100 + (-0.0007, 0.0014)$
$\text{Amp}_{\text{ABS,hf}}$	$0.2293 + (-0.0579, 0.0805)$	$0.1807 + (-0.0452, 0.0609)$
$\lambda_{\text{ABS,hf}}(mm)$	$0.2708 + (-0.0095, 0.0140)$	$0.1637 + (-0.0058, 0.0085)$

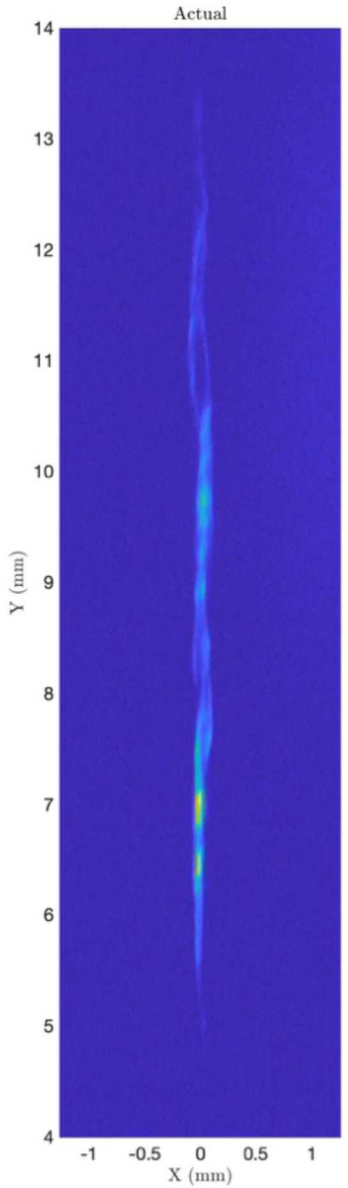

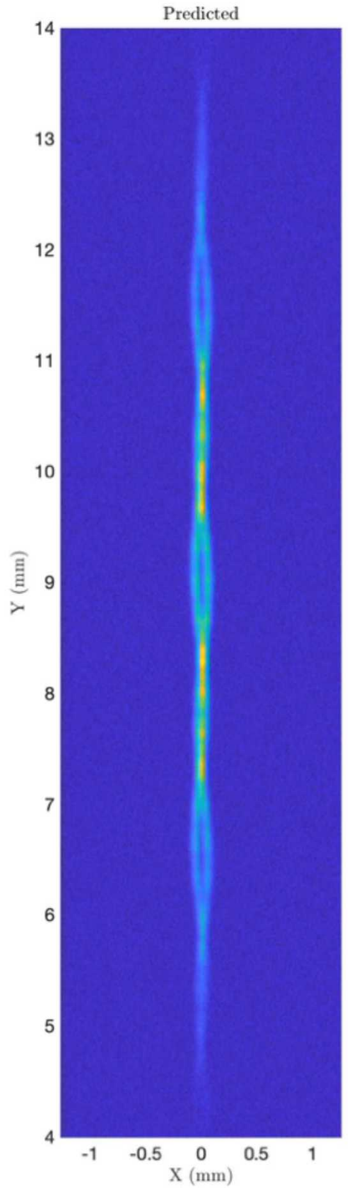

x

Shot Z3289 regression fit uncertainty

	Z3236	Z3289
θ_1	$0.0720 + (-0.0034, 0.0036)$	$0.0651 + (-0.0031, 0.0032)$
θ_2	$2.2335 + (-0.1425, 0.1546)$	$1.4954 + (-0.0950, 0.1013)$
θ_3	$2.1677 + (-0.3083, 0.3509)$	$3.9584 + (-0.5638, 0.6389)$
θ_4	$1.5327 + (-0.2560, 0.3003)$	$0.3120 + (-0.0509, 0.0622)$
θ_5	$0.0988 + (-0.0145, 0.0176)$	$0.1975 + (-0.0282, 0.0337)$
θ_6	$0.1756 + (-0.0568, 0.0838)$	$0.0116 + (-0.0037, 0.0058)$
θ_7	$6.8597 + (-3.1944, 5.8555)$	$79.2478 + (-36.5681, 68.3188)$
θ_8	$0.0286 + (-0.0107, 0.0175)$	$0.0136 + (-0.0051, 0.0084)$
θ_9	$0.2293 + (-0.0579, 0.0805)$	$0.1807 + (-0.0452, 0.0609)$
θ_{10}	$5.3522 + (-1.3159, 1.7144)$	$4.8469 + (-1.1991, 1.5604)$
θ_{11}	$0.4819 + (-0.4050, 0.4027)$	$2.0195 + (-0.4009, 0.4079)$

$\sigma_r(mm)$	$0.0720 + (-0.0034, 0.0036)$	$0.0651 + (-0.0031, 0.0032)$
$\sigma_z(mm)$	$2.2335 + (-0.1425, 0.1546)$	$1.4954 + (-0.0950, 0.1013)$
$\lambda_{helix}(mm)$	$2.8985 + (-0.4123, 0.4692)$	$1.5873 + (-0.2261, 0.2562)$
$R_{\text{helix}}(mm)$	$0.1275 + (-0.0512, 0.0811)$	$0.2111 + (-0.0853, 0.1359)$
$\text{Amp}_{\text{ABS,lf}}$	$0.1756 + (-0.0568, 0.0838)$	$0.0116 + (-0.0037, 0.0058)$
$\lambda_{\text{ABS,lf}}(mm)$	$0.2113 + (-0.0140, 0.0292)$	$0.0100 + (-0.0007, 0.0014)$
$\text{Amp}_{\text{ABS,hf}}$	$0.2293 + (-0.0579, 0.0805)$	$0.1807 + (-0.0452, 0.0609)$
$\lambda_{\text{ABS,hf}}(mm)$	$0.2708 + (-0.0095, 0.0140)$	$0.1637 + (-0.0058, 0.0085)$

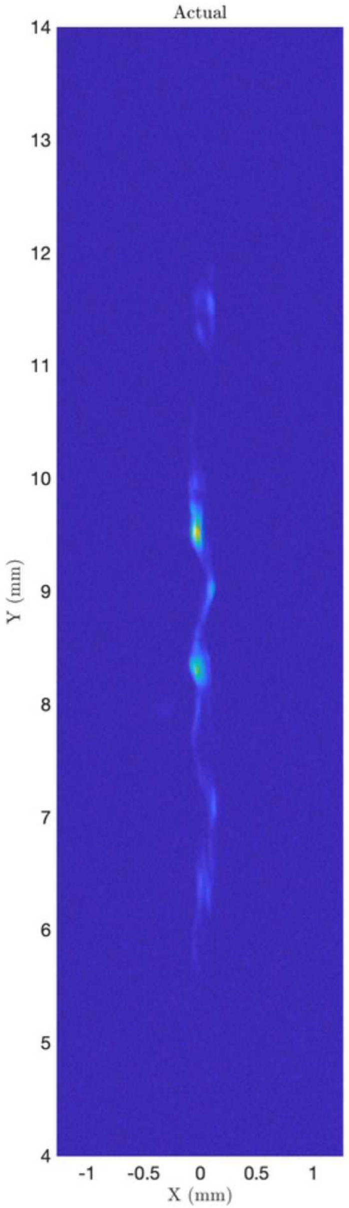

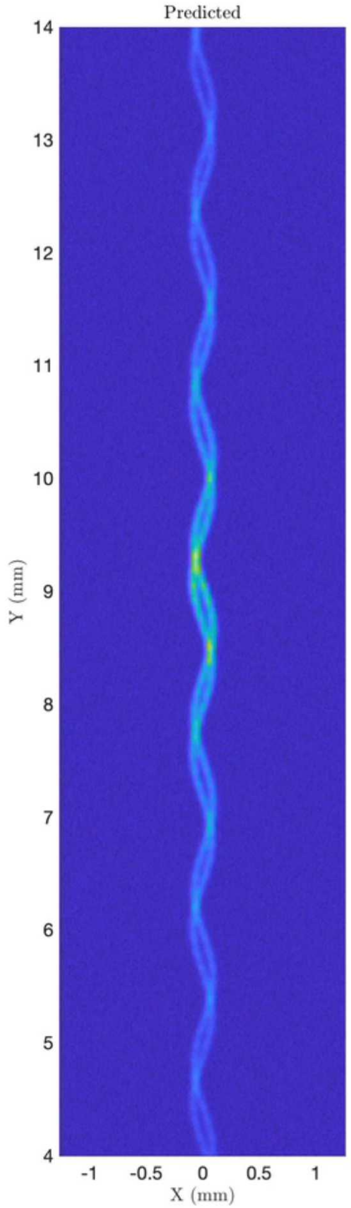

Fit to the two experimental images

	Z3236	Z3289
θ_1	$0.0720 + (-0.0034, 0.0036)$	$0.0651 + (-0.0031, 0.0032)$
θ_2	$2.2335 + (-0.1425, 0.1546)$	$1.4954 + (-0.0950, 0.1013)$
θ_3	$2.1677 + (-0.3083, 0.3509)$	$3.9584 + (-0.5638, 0.6389)$
θ_4	$1.5327 + (-0.2560, 0.3003)$	$0.3120 + (-0.0509, 0.0622)$
θ_5	$0.0988 + (-0.0145, 0.0176)$	$0.1975 + (-0.0282, 0.0337)$
θ_6	$0.1756 + (-0.0568, 0.0838)$	$0.0116 + (-0.0037, 0.0058)$
θ_7	$6.8597 + (-3.1944, 5.8555)$	$79.2478 + (-36.5681, 68.3188)$
θ_8	$0.0286 + (-0.0107, 0.0175)$	$0.0136 + (-0.0051, 0.0084)$
θ_9	$0.2293 + (-0.0579, 0.0805)$	$0.1807 + (-0.0452, 0.0609)$
θ_{10}	$5.3522 + (-1.3159, 1.7144)$	$4.8469 + (-1.1991, 1.5604)$
θ_{11}	$0.4819 + (-0.4050, 0.4027)$	$2.0195 + (-0.4009, 0.4079)$
$\sigma_r(mm)$	$0.0720 + (-0.0034, 0.0036)$	$0.0651 + (-0.0031, 0.0032)$
$\sigma_z(mm)$	$2.2335 + (-0.1425, 0.1546)$	$1.4954 + (-0.0950, 0.1013)$
$\lambda_{helix}(mm)$	$2.8985 + (-0.4123, 0.4692)$	$1.5873 + (-0.2261, 0.2562)$
$R_{\mathrm{helix}}(mm)$	$0.1275 + (-0.0512, 0.0811)$	$0.2111 + (-0.0853, 0.1359)$
$\mathrm{Amp}_{\mathrm{ABS,lf}}$	$0.1756 + (-0.0568, 0.0838)$	$0.0116 + (-0.0037, 0.0058)$
$\lambda_{\mathrm{ABS,lf}}(mm)$	$0.2113 + (-0.0140, 0.0292)$	$0.0100 + (-0.0007, 0.0014)$
$\mathrm{Amp}_{\mathrm{ABS,hf}}$	$0.2293 + (-0.0579, 0.0805)$	$0.1807 + (-0.0452, 0.0609)$
$\lambda_{\mathrm{ABS,hf}}(mm)$	$0.2708 + (-0.0095, 0.0140)$	$0.1637 + (-0.0058, 0.0085)$

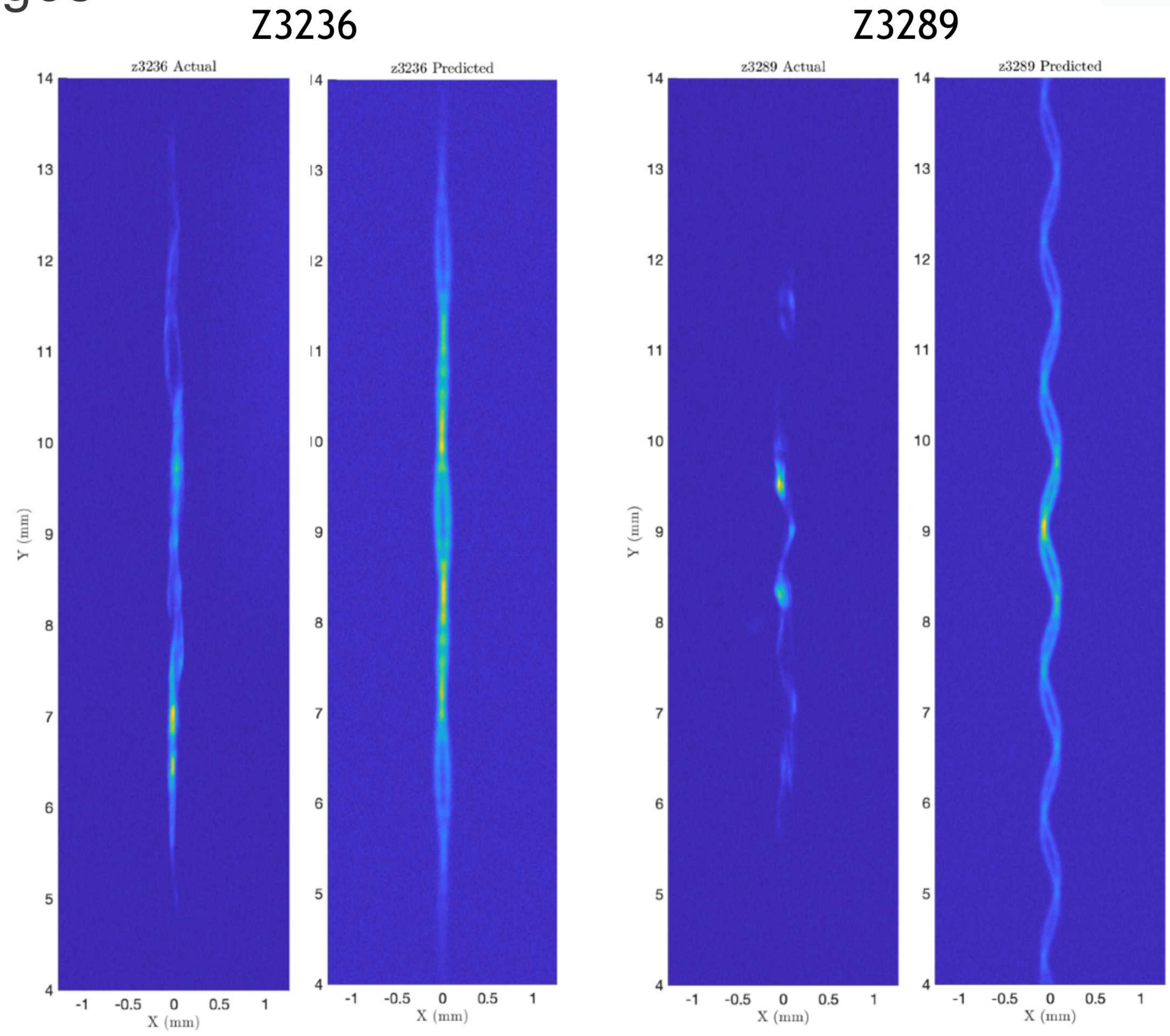

Comparative Results - coated AR9 vs uncoated AR6

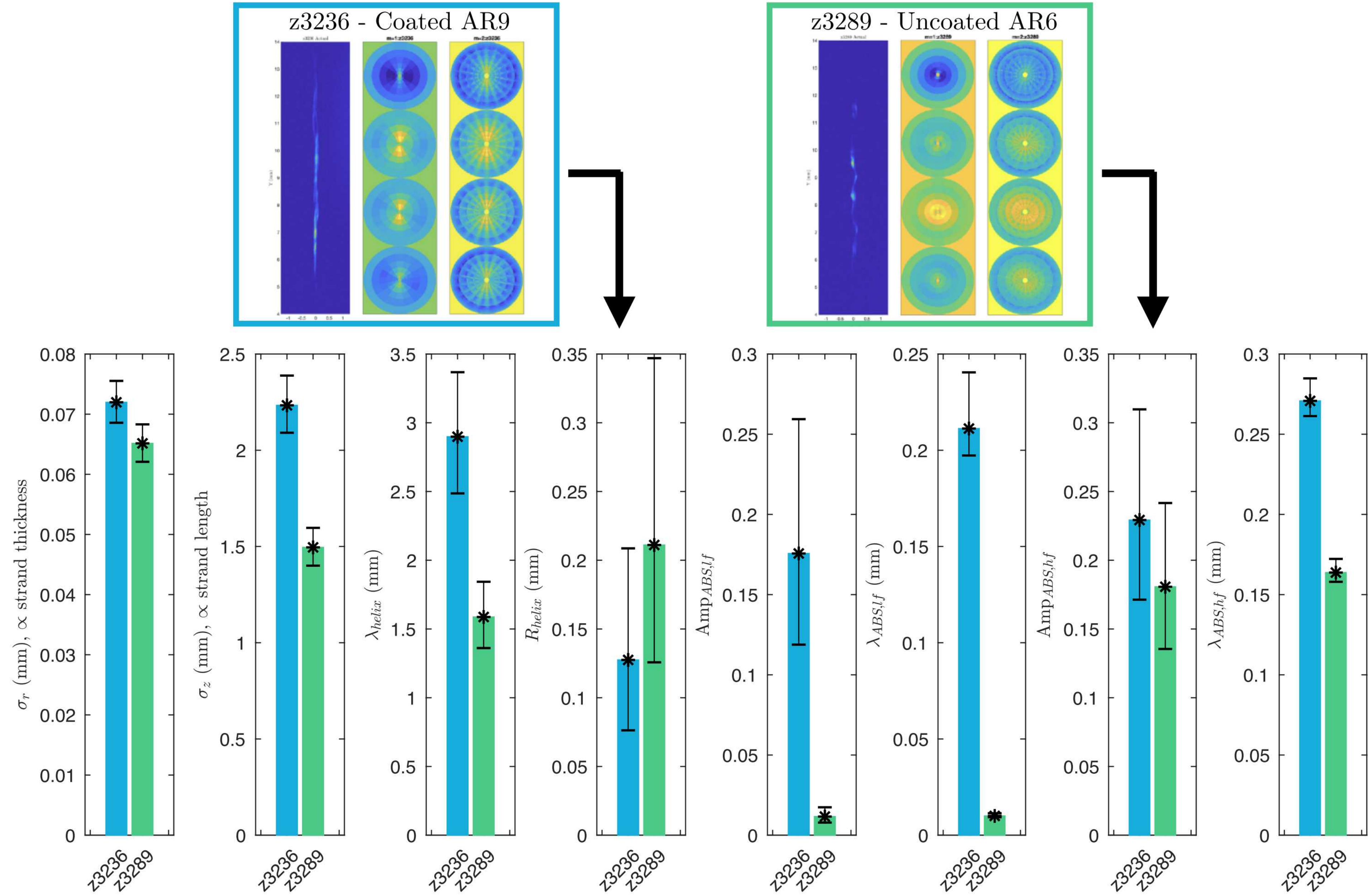

Optimization of MST

Model	**Validation Set R^2**
Base	0.9094
8192 training images	0.9237
$m = 1$	0.7238
2 rotations	0.8449
non-log_{10} on features	0.8752
Integrated intensity normalization	0.8849

Relationship of Generalized Master Equation to complexity (i.e., emergent behavior and self organization)

$p \equiv 1/\lambda$,canonical momentum, or quantum numbers

$$k(p,p') \equiv \frac{\bar{f}_2(p,p',t)}{\bar{f}_1(p,t)}$$

Generalized Master Equation $$\frac{\partial \bar{f}_1(p,t)}{\partial t} - \frac{\partial f_{\text{source}}(p)}{\partial t} \backsim \int dp' \; \bar{f}_1(p',t)\, k(p',p) - \bar{f}_1(p,t)\, k(p,p')$$

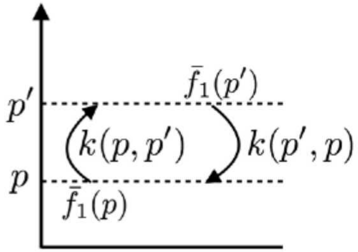

linear instability analysis

$$\bar{f}_1(p,t) \approx f_0(p,t) + \delta f(p,t) \quad \text{, where } \delta f/f_0 \ll 1$$

$$\Rightarrow \text{ dispersion relation, } D(p,t) = 0 \Rightarrow p = p_0(t)$$

$$p_0 = k + i\gamma$$

oscillation instability/stability

nonlinear steady state analysis

$$f_{\text{eq}}(p) \equiv \lim_{t\to\infty} \bar{f}_1(p,t)$$

$$\int dp' \; f_{\text{eq}}(p)\, k(p,p') - f_{\text{eq}}(p')\, k(p',p) \backsim \frac{\partial f_{\text{source}}(p)}{\partial t}$$

emergent behavior (e.g., 3D Kolmogorov scaling)

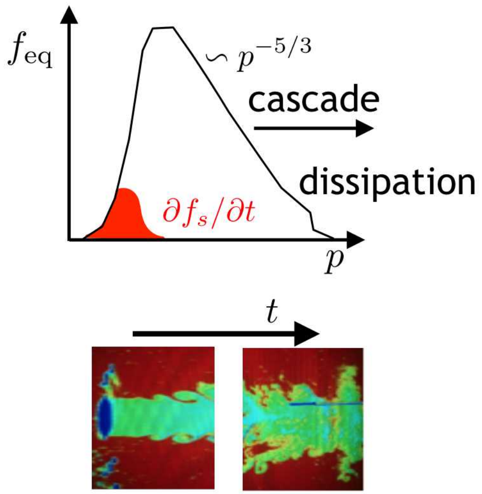

large scale self organization (e.g., 2D Navier-Stokes)

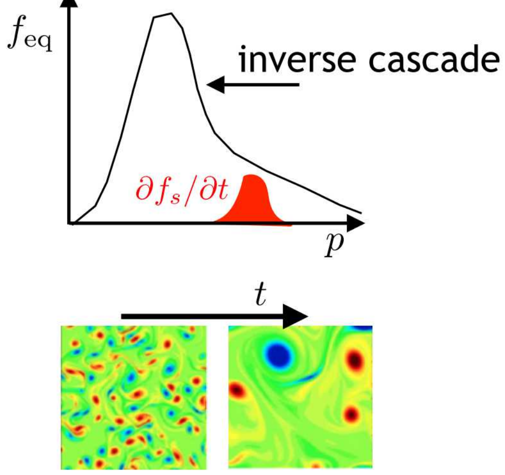

x

Why 3D MHD can exhibit a 2D Navier-Stokes inverse cascade with a resulting large scale, self organized, nonlinear, helical structure?

3D Navier-Stokes when constrained to 2D conserves total vorticity, relaxes energy while maintaining circulation

$$\text{total vorticity} = \int \nabla \times u \; d^2x$$

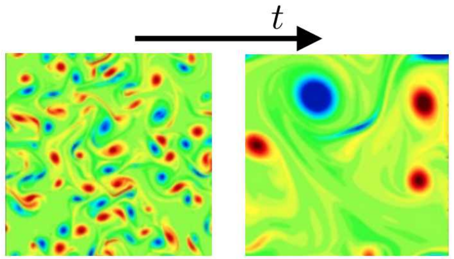

3D MHD when magnetized has total magnetic and cross helicity as a topological invariants, dissipates energy but must maintain helical twist

$$\text{total magnetic helicity} = \int A \cdot B \; d^3x$$

$$\text{total cross helicity} = \int v \cdot B \; d^3x$$

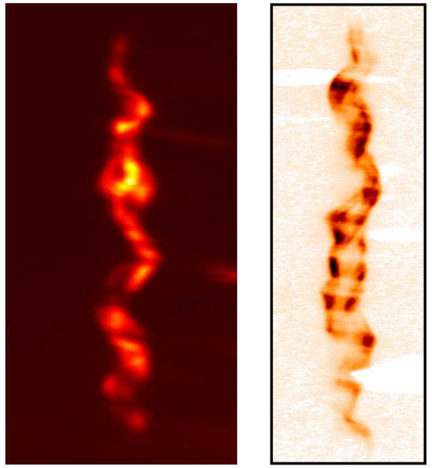

University of Michigan experiments track mode merger (inverse cascade) of liner structure

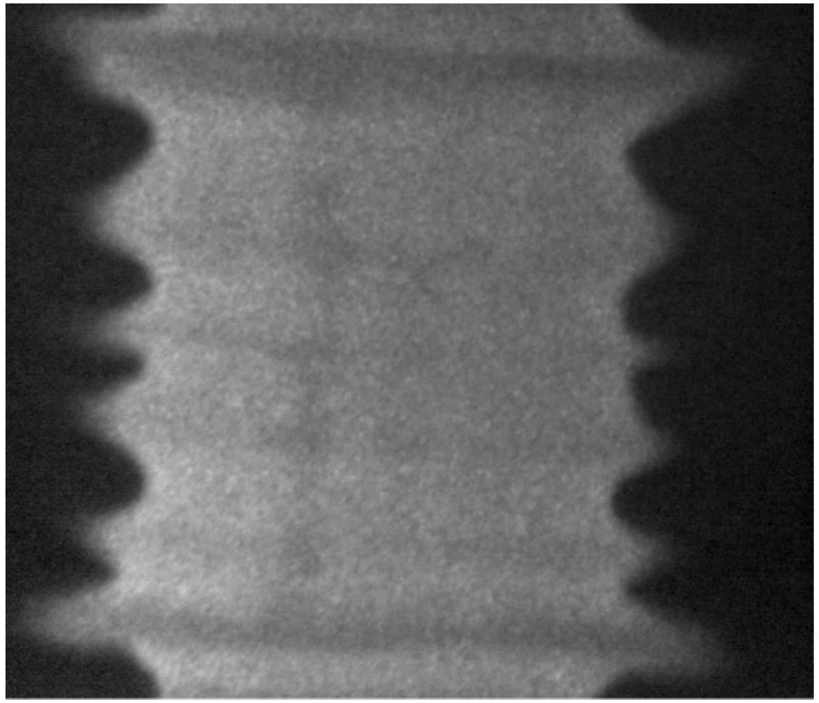

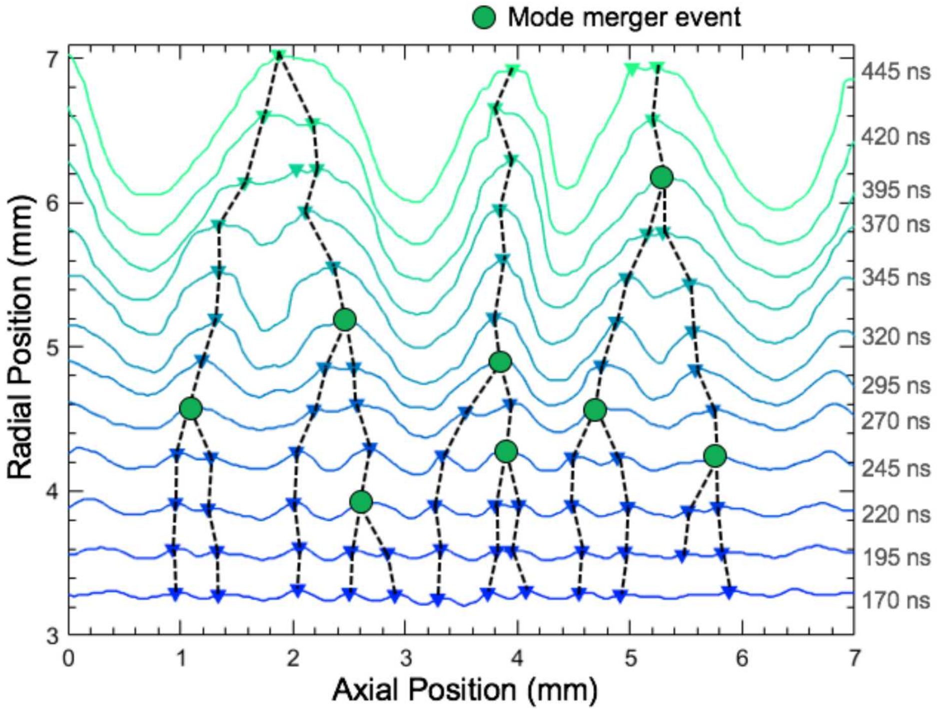

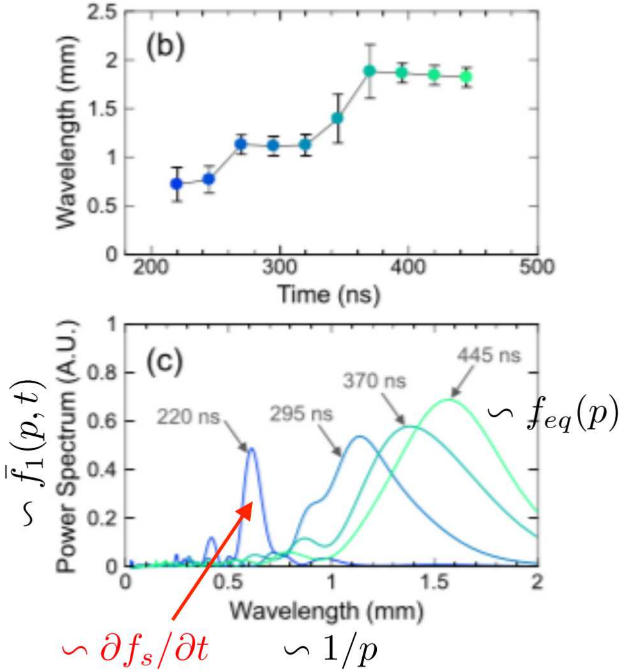

both with 1 T axial magnetic field and without

Axial magnetic field nonlinearly stabilizes liner perturbations into helical structure

Bz = 0

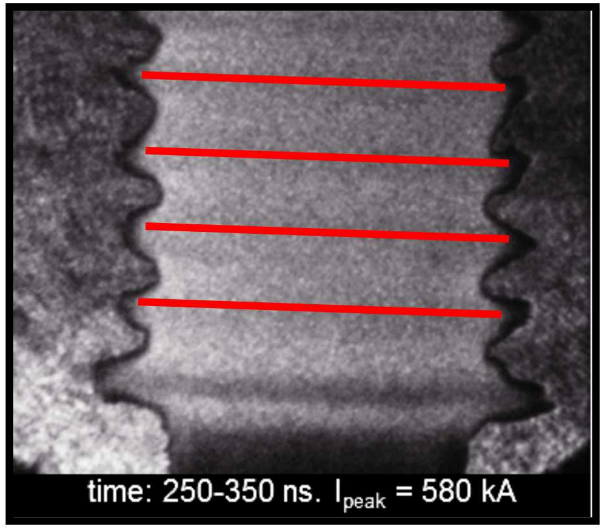

Bz = 1.1 T

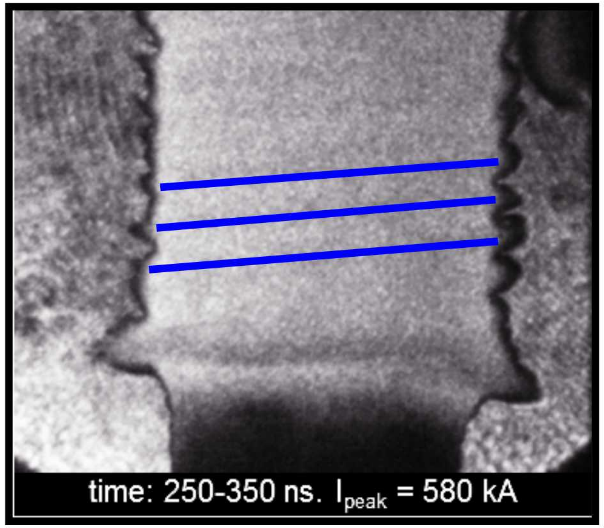

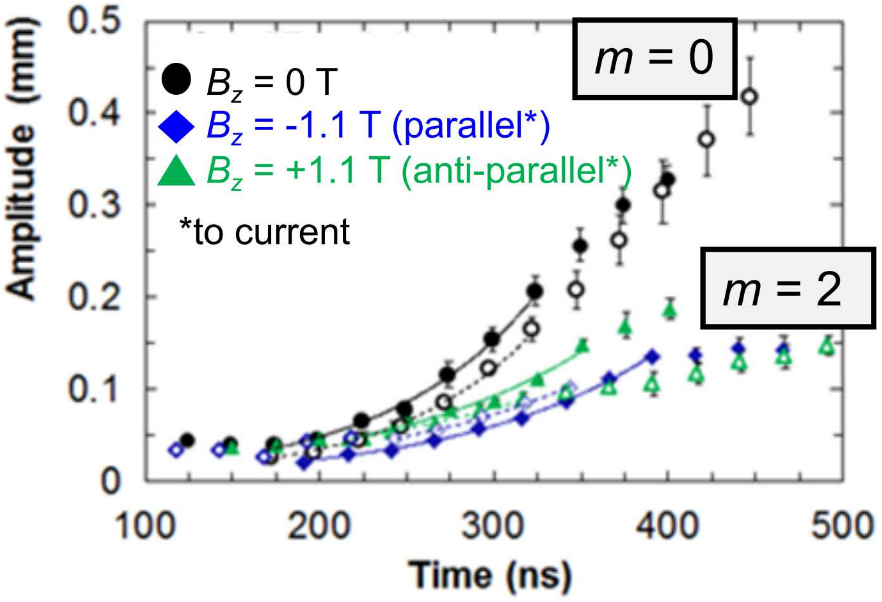

Unmagnetized
- Horizontal striations
- *m* = 0 sausage mode

Magnetized
- *m* = 2 helical mode
- Reduced amplitude
- Reverse B_z, striations also reverse

mode dependent on B, smaller than mode with largest linear growth rate

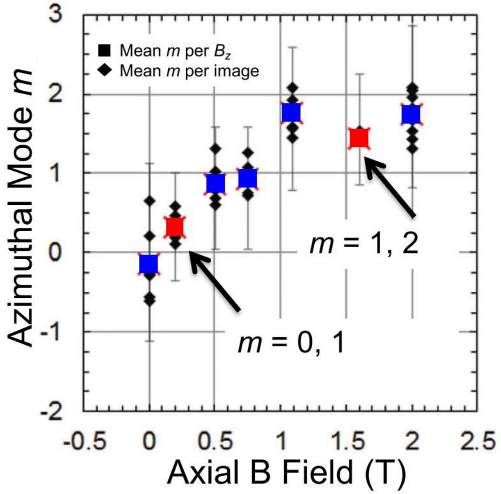

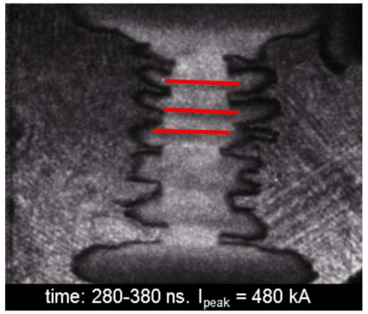

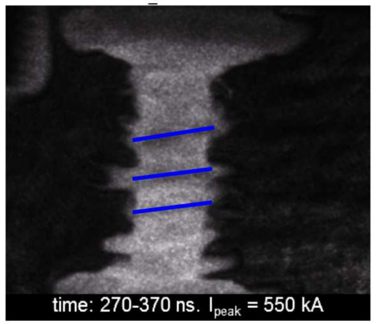

structure persists throughout implosion and bounce of liner

Evolution of distribution function to steady state

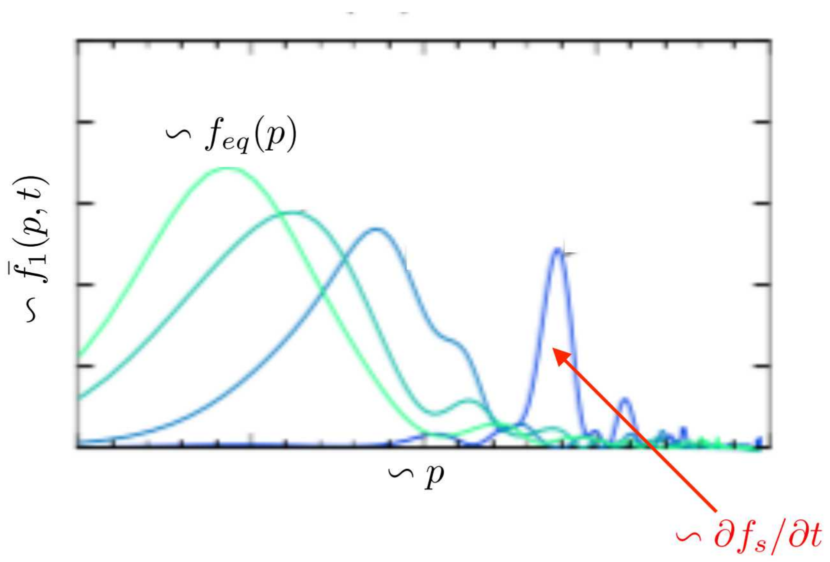

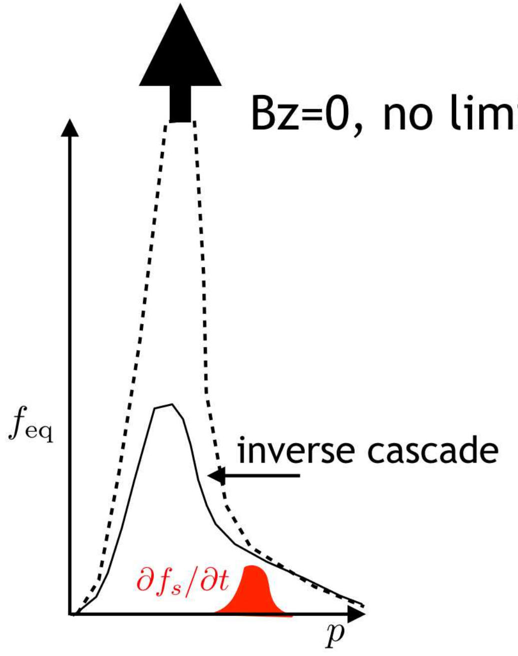

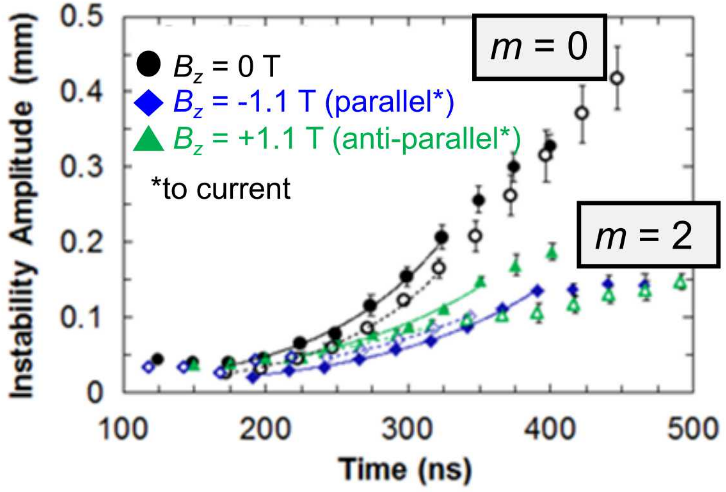

Main questions:

1. What is the steady state? (1st order MST, fixed point of 2nd order MST)
2. How does the physical system get there? (2nd order MST, kinetics)

Efficient, professional implementation of MST with visualization

- OpenSource Python package using Karas/TensorFlow, BluSky, that implements the 1D and 2D MST along with visualization to arbitrary order
- implementation is compatible with efficient inversion of the transformation because of the availability of derivatives (adjoints)
- implemented in time domain as a convolutional network, so that richer network structures can be investigated
- can be found at: https://github.com/enthought/sandia-blusky

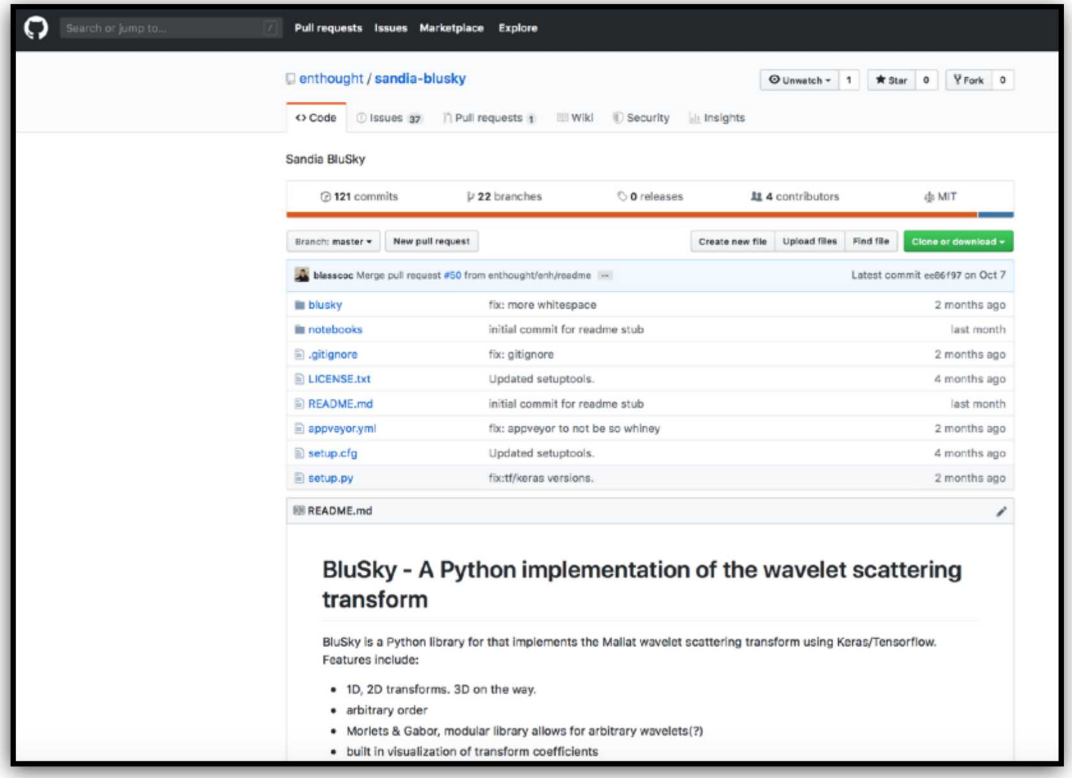

Backups

Technology to be presented

- Nonlinear physics vs. linear physics
  - linear instability vs. nonlinear stability
  - steady state structures (emergent behavior)
  - 2D inverse cascade vs 3D normal cascade
  - 2D Navier-Stokes with conserved vorticity and 3D MHD with topological helicity invariant
- Intuitive description of Mallat Scattering Transformation (MST)
- Connection of MST to nonlinear physics
  - Enhanced Wigner-Weyl transformation (manifold safe)
  - S-matrix (multiple scale, 1/momentum, scattering cross sections)
- Evidence for nonlinear stability, that is large scale emergent behavior in MagLIF implosions
  - mode merger
  - helical structure in liner with modes below linear mode with maximal growth rate
  - unexpected convergence to double helical structures with extreme CR>200
- Analysis of stagnation morphology with MST
  - advanced background subtraction
  - quantitative metric of morphology (that is, steady state nonlinear structure or emergent behavior)
  - regression to helical parameters with uncertainty (remarkably linear)

MST and kinetics (that is PDE solution)

- MST is advected with the diffeomorphism of a vector field on a manifold
  - leads to a set of "extended energies" or topological invariants, that are advected by the flow
- group symmetries can be built into the transformation
  - leads to additional constants advected by the flow
- MST is the "pull back" of the set of N particle distribution forms (i.e., density operators) using a modified version of the Wigner-Weyl transformation (mother wavelet with compact support replaces Fourier kernel, father wavelets are partition of unity)
  - Nth order MST is the Nth order Wigner function, that is N-particle correlation function
  - BBGKY hierarchy on manifolds gives evolution of the Nth order distribution function as an advection modified by a "collision operator" resulting from interaction with the N+1 particle (advective functional of the N+1 order distribution function)
- therefore, MST is the natural coordinate system to analyze statistical mechanics and kinetics
  - MST are constants for a steady state system allowing construction of the canonical ensemble following ideas of Jaynes
  - examples of generalized advective-collisional systems are:
    - Liouville equation
    - Boltzmann equation
    - Vlasov equation
    - MHD
    - Navier-Stokes
    - quantum field theory
    - quantum mechanics

x

Evidence for nonlinear helical structure of liner on Z, stabilized by axial magnetic field